# Regnase-1 Maintains Iron Homeostasis via the Degradation of Transferrin Receptor 1 and Prolyl-Hydroxylase-Domain-Containing Protein 3 mRNAs

AUTHOR(S):

Yoshinaga, Masanori; Nakatsuka, Yoshinari; Vandenbon, Alexis; Ori, Daisuke; Uehata, Takuya; Tsujimura, Tohru; Suzuki, Yutaka; Mino, Takashi; Takeuchi, Osamu

CITATION:

Yoshinaga, Masanori ...[et al]. Regnase-1 Maintains Iron Homeostasis via the Degradation of Transferrin Receptor 1 and Prolyl-Hydroxylase-Domain-Containing Protein 3 mRNAs. Cell Reports 2017, 19(8): 1614-1630

ISSUE DATE:

2017-05-23

URL:

http://hdl.handle.net/2433/224949

Article

Cell Reports

# Regnase-1 Maintains Iron Homeostasis via the Degradation of Transferrin Receptor 1 and Prolyl-Hydroxylase-Domain-Containing Protein 3 mRNAs

## Graphical Abstract

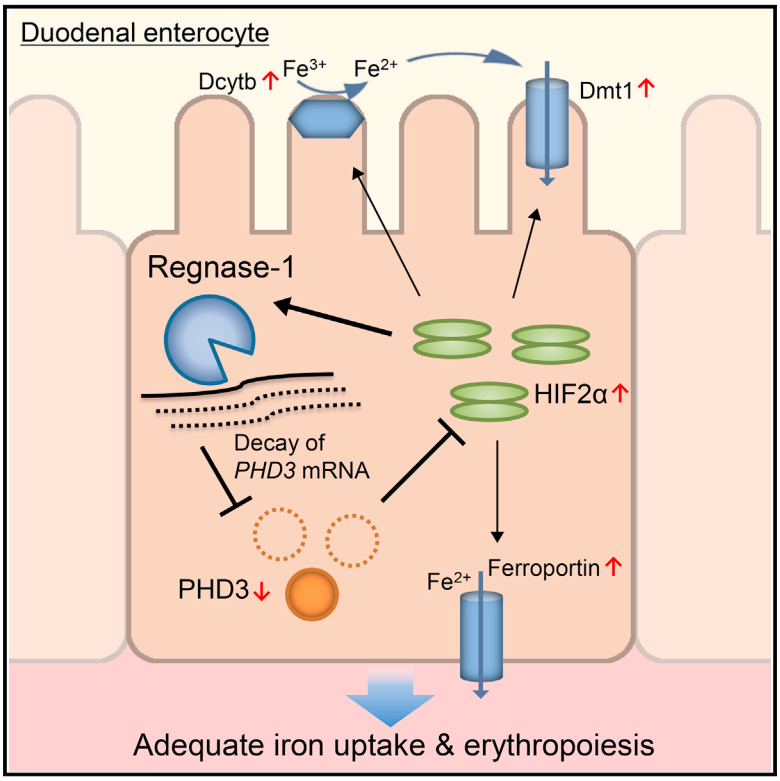


## Authors

Masanori Yoshinaga, Yoshinari Nakatsuka, Alexis Vandenbon, ..., Yutaka Suzuki, Takashi Mino, Osamu Takeuchi

## Correspondence

otake@infront.kyoto-u.ac.jp

## In Brief

Iron homeostasis is regulated by post-transcriptional mechanisms. Yoshinaga et al. demonstrate that an endoribonuclease, Regnase-1, destabilizes mRNAs related to iron metabolism, including TfR1 and PHD3. A positive feedback circuit of Regnase-1, PHD3, and HIF2α is critical for iron uptake in the duodenal epithelium and facilitates proper erythropoiesis.

## Highlights

- Regnase-1 destabilizes transferrin receptor 1 mRNAs via its ribonuclease activity
- Lack of Regnase-1 leads to the development of severe iron deficiency anemia in vivo
- Regnase-1 in the duodenal epithelium is required for iron homeostasis
- Regnase-1 destabilizes *PHD3* mRNA to facilitate duodenal iron uptake

## Accession Numbers

DRA003215

Yoshinaga et al., 2017, Cell Reports *19*, 1614–1630
May 23, 2017 
http://dx.doi.org/10.1016/j.celrep.2017.05.009

CellPress

Cell Reports
Article

# Regnase-1 Maintains Iron Homeostasis via the Degradation of Transferrin Receptor 1 and Prolyl-Hydroxylase-Domain-Containing Protein 3 mRNAs

Masanori Yoshinaga,[1,2] Yoshinari Nakatsuka,[1,2] Alexis Vandenbon,[3] Daisuke Ori,[1,6] Takuya Uehata,[1,2] Tohru Tsujimura,[4] Yutaka Suzuki,[5] Takashi Mino,[1,2] and Osamu Takeuchi[1,2,7,*]

[1]Laboratory of Infection and Prevention, Department of Virus Research, Institute for Frontier Life and Medical Sciences, Kyoto University, 53 Shogoin Kawara-cho, Sakyo-ku, Kyoto 606-8507, Japan
[2]Agency for Medical Research and Development-Core Research for Evolutional Medical Science and Technology (AMED-CREST), Japan Agency for Medical Research and Development, Tokyo 100-0004, Japan
[3]Immuno-Genomics Research Unit, WPI Immunology Frontier Research Center (IFReC), Osaka University, 3-1 Yamada-oka, Suita, Osaka 565-0871, Japan
[4]Department of Pathology, Hyogo College of Medicine, 1-1, Mukogawa-cho, Nishinomiya, Hyogo 663-8501, Japan
[5]Laboratory of Functional Genomics, Department of Medical Genome Sciences, Graduate School of Frontier Sciences, The University of Tokyo, 5-1-5 Kashiwanoha, Kashiwa-shi, Chiba 277-8562, Japan
[6]Present address: Laboratory of Molecular Immunobiology, Graduate School of Biological Sciences, Nara Institute of Science and Technology (NAIST), 8916-5 Takayama-cho, Ikoma, Nara 630-0192, Japan
[7]Lead Contact
*Correspondence: otake@infront.kyoto-u.ac.jp
http://dx.doi.org/10.1016/j.celrep.2017.05.009

## SUMMARY

**Iron metabolism is regulated by transcriptional and post-transcriptional mechanisms. The mRNA of the iron-controlling gene, transferrin receptor 1 (*TfR1*), has long been believed to be negatively regulated by a yet-unidentified endonuclease. Here, we show that the endonuclease Regnase-1 is critical for the degradation of mRNAs involved in iron metabolism in vivo. First, we demonstrate that Regnase-1 promotes *TfR1* mRNA decay. Next, we show that *Regnase-1*$^{-/-}$ mice suffer from severe iron deficiency anemia, although hepcidin expression is downregulated. The iron deficiency anemia is induced by a defect in duodenal iron uptake. We reveal that duodenal Regnase-1 controls the expression of PHD3, which impairs duodenal iron uptake via HIF2α suppression. Finally, we show that Regnase-1 is a HIF2α-inducible gene and thus provides a positive feedback loop for HIF2α activation via PHD3. Collectively, these results demonstrate that Regnase-1-mediated regulation of iron-related transcripts is essential for the maintenance of iron homeostasis.**

## INTRODUCTION

Iron metabolism is one of the most tightly controlled systems in mammals. Iron is required for essential biological functions, including oxygen delivery, but iron overload has deleterious effects, as seen in hemochromatosis. In order to circumvent iron deficiency and/or overload, iron uptake and storage is coordinately regulated by sensing systemic iron levels. Moreover, iron metabolism is closely linked to infection and inflammation, as well as systemic iron levels (Ganz and Nemeth, 2015; Muckenthaler et al., 2017).

Iron metabolism is regulated by both transcriptional and post-transcriptional mechanisms. Upon iron overload or inflammation, an iron hormone, hepcidin (encoded by *Hamp*), is transcribed in hepatocytes. Released hepcidin promotes the internalization and degradation of the sole known iron exporter in mammals, ferroportin (Fpn1, *Slc40a1*), leading to iron retention in the spleen and liver and to blockade of iron absorption in the duodenum (Drakesmith et al., 2015). Recently, it has also been revealed that hepcidin expression is controlled by an erythroid regulator, erythroferrone, produced by erythroblasts in response to erythropoietin (Kautz et al., 2014). Another essential regulator of iron homeostasis, especially for iron uptake in the duodenum, is the transcription factor hypoxia-inducible factor-2α (HIF2α). The HIF2α protein is stabilized by the inactivation of prolyl-hydroxylase-domain-containing proteins (PHD1-3, encoded by *Egln1-3*) and factor inhibiting HIF-1 (FIH), which are sensors for hypoxia and iron deficiency (Shah and Xie, 2014). Among these HIF hydroxylases, it has been suggested that PHD3 is relatively more effective in the degradation of HIF2α (Appelhoff et al., 2004). HIF2α forms a heterodimeric complex with aryl hydrocarbon receptor nuclear translocator (ARNT and HIF1β) and binds to the hypoxia-response element (HRE; typically 5′-RCGTG-3′, where R = A/G). HIF2α activates the transcription of iron-controlling genes that harbor HREs, including duodenal cytochrome B (*Dcytb* and *Cybrd1*), divalent metal transporter 1 (*Dmt1*, *Nramp2*, and *Slc11a2*), ferroportin (*Fpn1*), and presumably transferrin receptor 1 (*TfR1* and *Tfrc*), thereby promoting efficient duodenal iron uptake under iron-deficient conditions (Mastrogiannaki et al., 2009; Shah et al., 2009; Taylor et al., 2011).

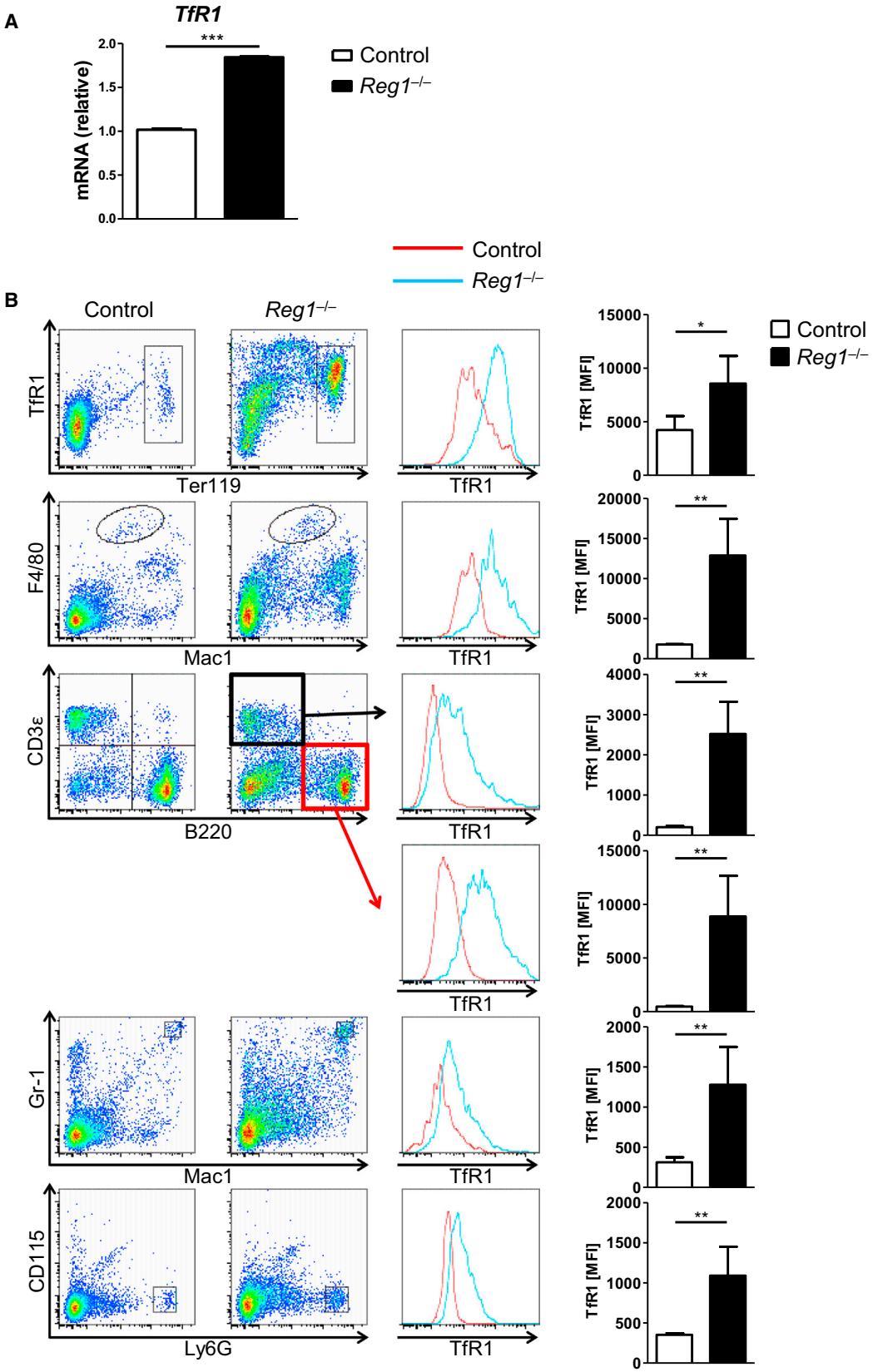


*(legend on next page)*

At the post-transcriptional level, mRNAs of the genes relating to iron transport and storage are widely regulated through the iron response element (IRE) iron response protein (IRP) axis (Kühn, 2015; Muckenthaler et al., 2017; Wilkinson and Pantopoulos, 2014). In their iron-deficient state, IRPs modulate the translation and stability of mRNAs through binding to IREs in the 5′ and 3′ UTR, respectively. In addition to regulation by IRPs, it has long been thought that *TfR1* mRNA is controlled by endogenous ribonucleases (Binder et al., 1994; Muckenthaler et al., 2017). However, the endonucleases responsible for the *TfR1* mRNA decay have not yet been identified.

We previously identified Regnase-1 (Reg1; also known as MCPIP1 or *Zc3h12a*) as an endonuclease that can destabilize a set of mRNAs, including interleukin-6 (*Il-6*) and *Il-12p40* (Matsushita et al., 2009; Mino et al., 2015). Reg1 is a cytoplasmic protein, which contains a CCCH-type zinc-finger motif and a N-terminal conserved domain that is similar to the PilT N terminus (PIN) domain and serves as a nuclease enzyme (Arcus et al., 2011; Matsushita et al., 2009). Unlike another CCCH-type zinc-finger protein, tristetraprolin (TTP), which recognizes and destabilizes mRNAs containing AU-rich elements (ARE) (Kafasla et al., 2014), Reg1 promotes the decay of mRNAs with stem-loop motifs in a translation-dependent manner (Mino et al., 2015). Genome-wide analysis has revealed that the canonical loop pattern of Reg1 target mRNAs is pyrimidine-purine-pyrimidine (e.g., UAU or UGU) (Mino et al., 2015). The essential role of Reg1 in immune responses has been intensively studied. *Reg1*$^{-/-}$ mice develop severe autoimmune disease, in which *Reg1*$^{-/-}$ T cells substantially contribute to the pathology (Iwasaki et al., 2011; Matsushita et al., 2009; Uehata et al., 2013). Reg1 is thus a pivotal post-transcriptional regulator in immune responses. Interestingly, we also found that mice deficient in Reg1 suffer from severe anemia (Matsushita et al., 2009). However, the mechanisms by which mice with Reg1 deficiency develop anemia have remained obscure.

In the current study, we investigated the role of Reg1 in iron metabolism. We found augmented expression of TfR1 in Reg1-deficient cells, resulting from a lack of direct destabilization of *TfR1* mRNA by Reg1. Analysis of knockout mice further revealed that the ribonuclease activity of Reg1 destabilized the mRNA of another iron-controlling gene, *PHD3*, contributing to efficient iron uptake in the duodenum. Moreover, the expression of Reg1 in the duodenum was controlled under conditions of iron deficiency through the activity of HIF2α. Thus, Reg1 forms a critical positive feedback loop for HIF2α activation to promote duodenal iron uptake.

## RESULTS

### *TfR1* Expression Is Elevated in the Absence of Reg1

To explore Reg1 target genes associated with the regulation of iron homeostasis, we first analyzed the previous microarray dataset of *Reg1*$^{-/-}$ macrophages cultured in standard medium (Matsushita et al., 2009). We found that *TfR1* was upregulated under deficiency of Reg1 (Table S1). Since the expression of TfR1 is highly affected by intracellular iron levels, we depleted iron in the culture medium by adding an iron chelator, deferoxamine mesylate (DFO). In this iron-depleted medium, *TfR1* mRNA expression was significantly higher in *Reg1*$^{-/-}$ peritoneal exudate cells (PECs) than in those from wild-type mice (Figure 1A).

Also, to confirm that this upregulation of TfR1 is ubiquitous among various cell types, we conducted flow cytometry analysis to assess the expression in splenocytes of *Reg1*$^{-/-}$ mice. In the absence of Reg1, significantly higher levels of TfR1 were detected not only in cells relating to iron homeostasis, including Ter119$^{+}$ erythroblasts and CD11b$^{lo}$F4/80$^{+}$ red pulp macrophages, but also in CD3ε$^{+}$ T cells, B220$^{+}$ B cells, Gr-1$^{+}$Mac1$^{+}$ myeloid cells, and Ly6G$^{+}$CD115$^{-}$ neutrophils (Figure 1B), suggesting a cell-type-independent regulation of TfR1 expression. TfR1 expression was significantly higher in *Reg1*$^{-/-}$ splenic cells, even after iron treatment in vitro and in vivo (Figures S1A and S1B). Taken together, these results indicate that TfR1 expression is negatively regulated by Reg1 in various hematopoietic cells.

### *TfR1* mRNA Is Directly Regulated by Reg1

The upregulation of TfR1 in the absence of Reg1 prompted us to test whether Reg1 directly regulates TfR1 via its ribonuclease activity. qRT-PCR analysis revealed that *TfR1* mRNA was stabilized in the absence of Reg1 compared to the control after treatment with the transcription inhibitor, actinomycin D (ActD) (Figure 2A). Reciprocally, under overexpression of Reg1, the decay rate of *TfR1* mRNA was accelerated compared to the control (Figure 2B). We next asked whether Reg1 is associated with *TfR1* mRNA and performed RNA immunoprecipitation (RIP)-qPCR analysis. We found that *TfR1* mRNA, but not 18S rRNA, co-precipitated with a Reg1-D141N nuclease-inactive mutant (Figure 2C), indicating Reg1 directly associates with *TfR1* mRNA.

Next, to test whether the 3′ UTR of *TfR1* mRNA is sufficient for Reg1-mediated mRNA decay, we inserted the full-length 3′ UTR of mouse *TfR1* mRNA (mTfR1-3′ UTR-full) into luciferase reporter constructs (pGL3) and assessed the luciferase activity under overexpression of Reg1 (Figure 2D). We found that Reg1 overexpression reduced the luciferase activity of pGL3-mTfR1-3′ UTR-full compared to control (Figure 2E). Then, to further investigate the regions critical for conferring Reg1 responsiveness, we made a series of pGL3s containing a part of the 3′ UTR of *TfR1* mRNA (Figure 2D). The *TfR1* 3′ UTR harbors five evolutionarily conserved IREs, and the endonucleolytic cleavage site in *TfR1* 3′ UTR is believed to be located among IREs (Binder et al., 1994). Indeed, the luciferase activity of pGL3-mTfR1-3′ UTR-(768–1,525), which contains all IREs, decreased under

**Figure 1. Elevation of TfR1 in the Absence of Reg1**

(A) Mouse PECs from *Reg1*$^{-/-}$ mice were incubated in medium supplemented with 100 μM DFO. After overnight incubation, total RNA was extracted, and levels of *TfR1* mRNA were measured by qRT-PCR. Data are representative of five independent experiments.

(B) Total splenocytes from *Reg1*$^{-/-}$ mice were analyzed using flow cytometry as indicated (left). Data are representative of four biological replicates. Histograms of TfR1 intensity and TfR1 mean fluorescence intensity (MFI) in each gated population (n = 4) (right).

Data are expressed as mean ± SD of triplicates (A) or biological replicates (B). *p < 0.05, **p < 0.01, ***p < 0.001 (Student's t test). See also Figure S1 and Table S1.

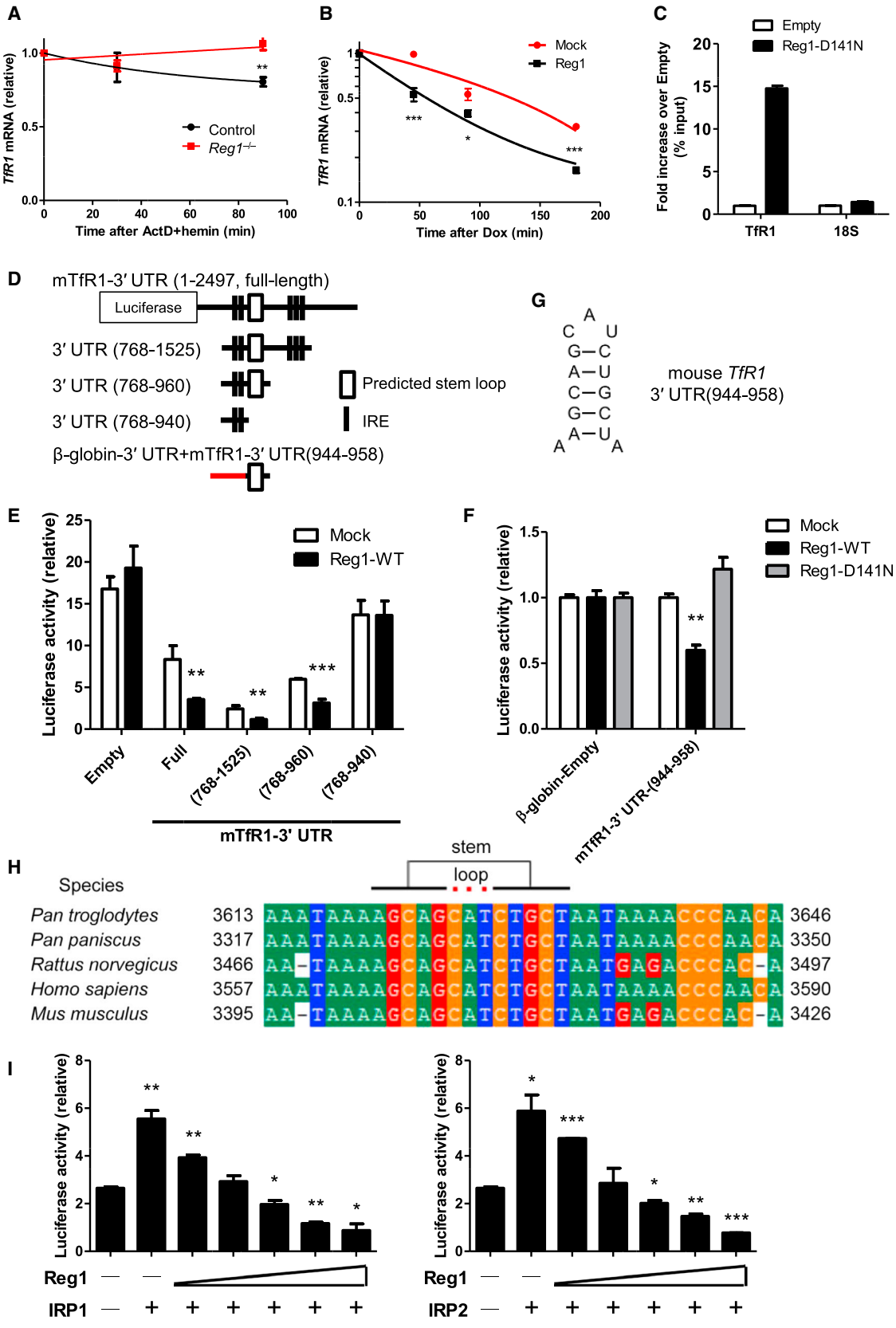


*(legend on next page)*

overexpression of wild-type Reg1 (Figure 2E). Furthermore, whereas the luciferase activity of pGL3-mTfR1-3′ UTR-(768–940) was not altered by co-expression of Reg1, the activity of pGL3-mTfR1-3′ UTR-(768–960) decreased (Figure 2E), suggesting the sequence between 940 and 960 is critical for regulating *TfR1* mRNA decay. The sequence between 944 and 958 in the 3′ UTR of mouse *TfR1* mRNA is in close proximity to an IRE and predicted to form a stem-loop structure with a pyrimidine-purine-pyrimidine loop (Figure 2G), which is consistent with the consensus Reg1 recognition motif (Mino et al., 2015). The addition of this sequence to the end of β-globin 3′ UTR reduced luciferase activity in the presence of wild-type Reg1, but not the D141N mutant, indicating that Reg1 acts as a nuclease to destabilize *TfR1* 3′ UTR (Figure 2F). The minimal sequence between 944 and 958 in mouse *TfR1* mRNA is identical to that of human and evolutionarily conserved among a variety of mammals (Figure 2H), suggesting a functional significance for the regulation of *TfR1* mRNA.

Next, we further investigated the relationship between Reg1 and IRPs by co-transfecting cells with a luciferase reporter containing full-length *TfR1* 3′ UTR and the expression vectors of Reg1 and IRPs. Luciferase activity was reduced when the dose of the Reg1 expression vector was increased (Figure 2I), indicating that Reg1 has the potential to counteract mRNA stabilization by IRP1 and IRP2. These results collectively support the view that Reg1 is an endonuclease destabilizing *TfR1* mRNA via its 3′ UTR.

### *Reg1*$^{-/-}$ Mice Show Severe Iron Deficiency Anemia

To further investigate the role of Reg1 in iron homeostasis, we next assessed the effect of the genetic ablation of Reg1 in mice. In our previous study, we showed that *Reg1*$^{-/-}$ mice suffered from severe anemia (Matsushita et al., 2009). This finding was corroborated by the observation that hematological parameters of *Reg1*$^{-/-}$ mice, including red blood cell (RBC) numbers, hemoglobin (HGB), and hematocrit (HCT) levels, progressively deteriorated with maturation (Figure 3A). Also, non-heme iron levels were markedly lower in serum and iron-storage tissues, including the liver and spleen, in *Reg1*$^{-/-}$ mice (Figures 3B and 3C). Tissue iron staining also confirmed low accumulation of iron in the spleen and liver in *Reg1*$^{-/-}$ mice (Figure 3D), indicating *Reg1*$^{-/-}$ mice also suffered from severe iron deficiency. Moreover, the mRNA levels of hepcidin were almost undetectable in the liver of *Reg1*$^{-/-}$ mice (Figure 3E), although these mice developed spontaneous severe autoimmune disease and inflammation. We also found that the unbound iron-binding capacity (UIBC) and total iron-binding capacity (TIBC) significantly increased in *Reg1*$^{-/-}$ mice, while transferrin saturation decreased in *Reg1*$^{-/-}$ mice (Figure 3F), supporting the notion that this anemia is iron deficiency anemia rather than anemia of inflammation. Moreover, we found that the expression of erythropoietin was augmented in *Reg1*$^{-/-}$ kidney (Figure 3G), consistent with decreased HGB levels. Furthermore, we examined erythroferrone expression in bone marrow cells and spleen from *Reg1*$^{-/-}$ mice and found that expression was upregulated in these organs (Figure 3H), which might be one possible explanation for hepcidin downregulation. Taken together, these findings indicate that *Reg1*$^{-/-}$ mice spontaneously develop iron deficiency anemia, while hepcidin expression is downregulated.

Next, we analyzed gene expression in the liver of *Reg1*$^{-/-}$ mice to examine if Reg1 expressed in the liver controls iron uptake, thereby inducing iron deficiency anemia. We found that mRNA levels of the genes responsible for iron uptake in the liver, including *TfR1* and *Dmt1*, were significantly upregulated in *Reg1*$^{-/-}$ liver (Figure S2A), consistent with their regulation by the IRE-IRP system. Therefore, we next analyzed the IRP expression in the liver and found that IRP2 protein accumulated in *Reg1*$^{-/-}$ liver (Figure S2B). IRP2 protein accumulation was also observed in *Reg1*$^{-/-}$ heart (Figure S2B), suggesting that this upregulation was observed in multiple organs in *Reg1*$^{-/-}$ mice. Consistent with the accumulation of IRP2 protein, we found that ferritin expression was downregulated in *Reg1*$^{-/-}$ liver at the protein level (Figure S2D). The upregulation of IRP2 protein is not due to post-transcriptional regulation of *IRP* mRNA by Reg1, because the expression of *IRP1* or *IRP2* mRNA was not augmented in Reg1-deficient tissues (Figure S2F). These findings suggest that the IRP activation is induced by cytosolic iron depletion in the liver under Reg1 deficiency, which is consistent with the severe iron deficiency found in *Reg1*$^{-/-}$ mice. Therefore, it is unlikely that the aberrant regulation of the IRE-IRP system in the liver is the primary cause of iron deficiency anemia in *Reg1*$^{-/-}$ mice.

It is known that autoimmune disease can induce anemia via several mechanisms (Weiss and Goodnough, 2005; Zhou et al., 2013). Given that *Reg1*$^{-/-}$ mice develop severe

**Figure 2. *TfR1* mRNA Is Directly Regulated by Reg1**

(A) PECs harvested from *Reg1*$^{-/-}$ mice were incubated overnight in the medium supplemented with DFO (100 μM). The cells were then treated with ActD (1 μg/mL) and hemin (100 μM) for the indicated times. Total RNA was extracted, and the levels of *TfR1* mRNA were measured by qRT-PCR.

(B) HEK293 Tet-Off cells were co-transfected with pTREtight-mTfR1-CDS-3′ UTR, together with the Reg1 expression vector or the control (mock). Total RNA was extracted after doxycycline hyclate (Dox; 1 μg/mL) treatment, and the levels of *TfR1* mRNA were measured by qRT-PCR.

(C) HEK293T cells were transfected with mutant Reg1 (Reg1-D141N) expression vector or the control (empty). RNA-protein complexes were immunoprecipitated, and the levels of *TfR1* mRNA and 18S rRNA were measured by qRT-PCR.

(D–F) HEK293T cells were co-transfected with a series of luciferase reporter plasmids (D) and the expression plasmids for wild-type Reg1 (Reg1-WT), Reg1-D141N, or empty plasmid as a control (mock). After 48 hr of incubation, luciferase activity of cell lysates was determined (E and F).

(G) The predicted stem-loop structure of mouse *TfR1* 3′ UTR-(944–958).

(H) Alignment of the conserved sequence in *TfR1* 3′ UTR among mammals.

(I) HEK293T cells were co-transfected with either IRP1 or IRP2 expression vector, together with pGL3-hTfR1-3′ UTR-full, and the Reg1 expression plasmid or the control.

Data are representative of two (C) or three (A, B, E, F, and I) independent experiments. Data are expressed as mean ± SD of triplicates (A–C and E) or duplicates (F and I). *$p < 0.05$, **$p < 0.01$, ***$p < 0.001$ (Student's t test).

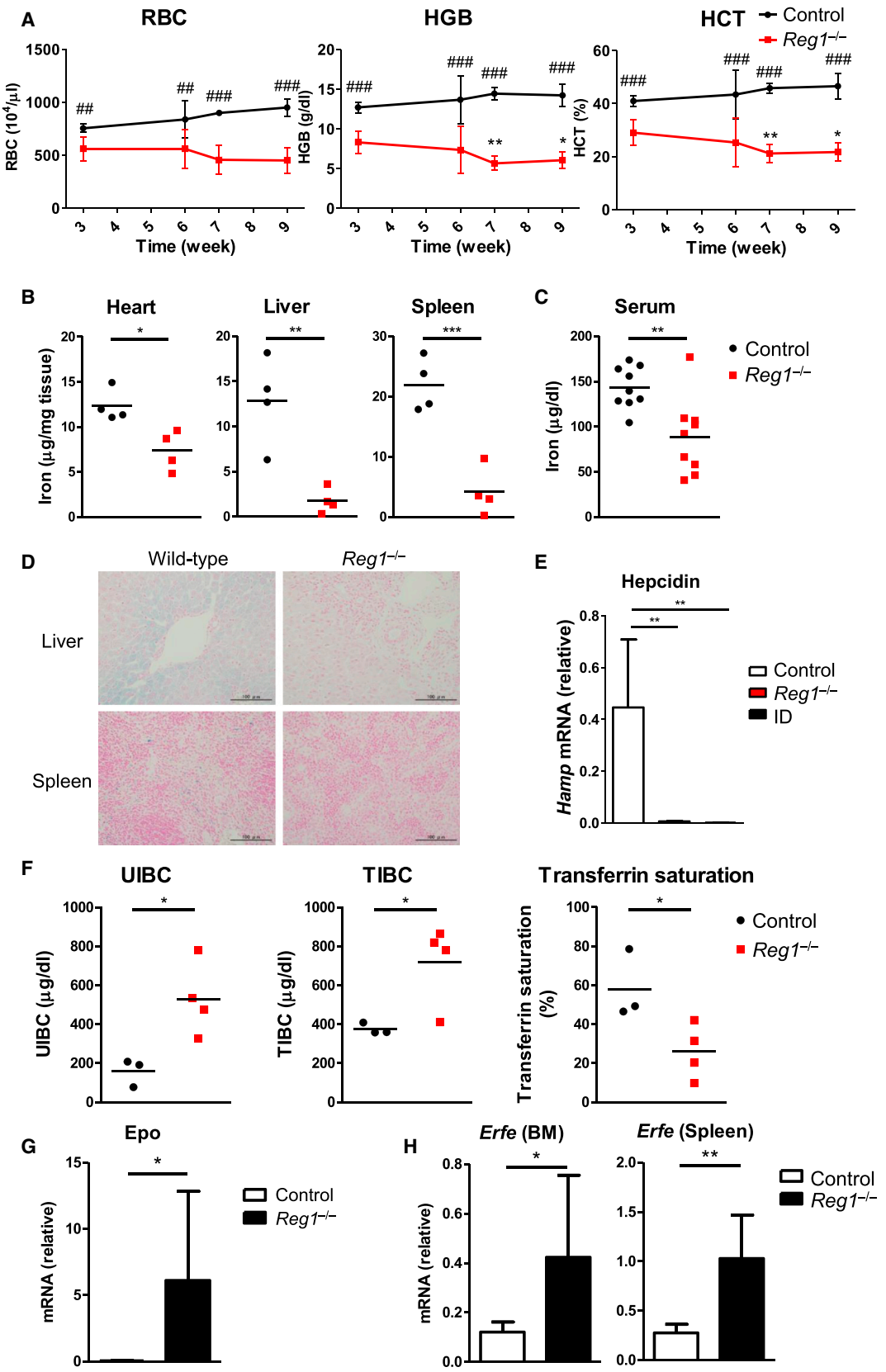


(legend on next page)

autoimmune disease due to T cell activation (Matsushita et al., 2009; Uehata et al., 2013), aberrant activation of the adaptive immune system might induce such anemia in *Reg1*$^{-/-}$ mice. To exclude this possibility, we generated mice deficient in Rag2 and Reg1 (*Rag2*$^{-/-}$*Reg1*$^{-/-}$ mice), in which mature lymphocytes as well as immunoglobulins are absent. Indeed, white blood cell numbers were significantly lower in *Rag2*$^{-/-}$*Reg1*$^{-/-}$ mice than in *Reg1*$^{-/-}$ mice (Figure S3A). On the other hand, hematological parameters (including RBC, HGB, and HCT levels; and mean corpuscular HGB concentration [MCHC]) and tissue iron levels were significantly lower in *Rag2*$^{-/-}$*Reg1*$^{-/-}$ mice than in control mice but comparable to those of *Reg1*$^{-/-}$ mice (Figures S3A and S3B). These findings indicate that lymphocyte deficiency does not ameliorate iron deficiency anemia in *Reg1*$^{-/-}$ mice. Autoimmune gastritis is also known to be a cause of anemia, since the stomach lining is crucial for the facilitation of vitamin $B_{12}$ and iron absorption. However, histopathological analysis of gastrointestinal tracts, including the stomach from *Reg1*$^{-/-}$ and *Rag2*$^{-/-}$*Reg1*$^{-/-}$ mice, revealed little evidence of inflammation, such as lymphocyte infiltration (Figure S3C), indicating that the anemia was not caused by gastritis. We also performed such histopathological analyses on other organs and found infiltration of inflammatory cells in *Reg1*$^{-/-}$ and *Rag2*$^{-/-}$*Reg1*$^{-/-}$ liver, although this change did not lead to the upregulation of hepcidin mRNA in *Rag2*$^{-/-}$*Reg1*$^{-/-}$ liver (Figures S3C and S3D). Collectively, these results suggest that Reg1 directly controls iron homeostasis independent of inflammation.

## Reg1 Is Required for Duodenal Iron Uptake

Next, we further investigated the mechanisms of iron deficiency anemia in *Reg1*$^{-/-}$ mice. Since there is no excretory pathway for iron under physiological conditions, pathologic iron loss and/or impaired iron absorption can be the cause of iron deficiency. As for iron loss, no obvious bleeding, including gastrointestinal hemorrhage, was observed (data not shown). Therefore, we next focused on the duodenum, which is a region critical for the uptake of iron in the diet. Tissue iron levels were significantly lower in *Reg1*$^{-/-}$ duodenum (Figure 4A). Histological analysis of iron staining confirmed remarkable tissue-iron reduction in the duodenal epithelium of *Reg1*$^{-/-}$ mice and *Rag2*$^{-/-}$*Reg1*$^{-/-}$ mice (Figures 4B and S3C). These findings indicate that the duodenum could not access dietary iron efficiently in *Reg1*$^{-/-}$ mice.

To investigate the role of Reg1 in the duodenum, we next generated mice lacking Reg1 specifically in the intestinal epithelium (*Reg1*$^{fl/fl}$*Villin-Cre*$^{+}$ mice). The levels of *Reg1* mRNA in the duodenal epithelial cells of *Reg1*$^{fl/fl}$*Villin-Cre*$^{+}$ mice decreased substantially (Figure 4C). First, we asked whether these mice show any evidence of inflammation. Histological, qRT-PCR, and flow cytometric analyses revealed no spontaneous immune activation in *Reg1*$^{fl/fl}$*Villin-Cre*$^{+}$ mice, including colitis (Figures S4A–S4E). The absence of spontaneous immune activation in *Reg1*$^{fl/fl}$*Villin-Cre*$^{+}$ mice makes them suitable for the study of iron metabolism.

Next, we asked whether intestinal Reg1 plays a role in iron homeostasis. *Reg1*$^{fl/fl}$*Villin-Cre*$^{+}$ mice showed lower HGB and HCT levels and lower mean corpuscular volume (MCV) and MCHC at the age of 4–6 weeks (Figure 4D). Tissue iron levels in the liver and spleen were also significantly lower in 4- to 6-week-old *Reg1*$^{fl/fl}$*Villin-Cre*$^{+}$ mice than in control mice (Figure 4E). Furthermore, consistent with the low tissue iron levels, hepcidin expression levels in the liver were significantly lower in *Reg1*$^{fl/fl}$*Villin-Cre*$^{+}$ mice than in control mice (Figure 4F). Taken together, these findings demonstrate that Reg1 expressed in intestinal epithelium cells regulates iron homeostasis and erythropoiesis in vivo.

These observations led us to hypothesize that impaired duodenal iron absorption is the cause of iron deficiency anemia in *Reg1*$^{-/-}$ mice. To test this hypothesis, we analyzed mice that were intraperitoneally injected with saccharated ferric oxide (Figure S5A). As expected, iron administration into mice deficient in Reg1 partially restored tissue iron levels and HGB levels (Figures 4G, 4H, and S5B). Also, hepcidin expression in *Reg1*$^{-/-}$ liver became comparable to that of untreated wild-type mice, presumably in response to the restoration of iron levels (Figure S5C), suggesting that the regulation of hepcidin expression is intact in *Reg1*$^{-/-}$ mice. In the aggregate, these findings suggest that impaired duodenal iron absorption contributed to altered iron homeostasis in *Reg1*$^{-/-}$ mice.

## Reg1 Deficiency in the Duodenum Does Not Induce Ferritin Expression

It is well known that upregulation of ferritin H due to IRP inactivation in the duodenum leads to iron deficiency (Galy et al., 2013; Kühn, 2015; Vanoaica et al., 2010). However, we did not observe the upregulation of ferritin H or IRP inactivation in *Reg1*$^{-/-}$ duodenum (Figures S2C and S2E). Therefore, these findings rule out

**Figure 3. *Reg1*$^{-/-}$ Mice Develop Severe Iron Deficiency Anemia**

(A) Hematological parameters of *Reg1*$^{-/-}$ mice at indicated time points (n = 4–10).
(B) Iron levels of each organ from *Reg1*$^{-/-}$ mice (n = 4).
(C) Serum iron levels of *Reg1*$^{-/-}$ mice (n = 9).
(D) Berlin blue stain of the liver (top) and the spleen (bottom) from *Reg1*$^{-/-}$ mice to detect tissue iron. Representative images of each genotype are shown.
(E) Hepcidin mRNA expression levels in the liver of control, *Reg1*$^{-/-}$ and iron-deficient (ID) mice (n = 4–5). Control and *Reg1*$^{-/-}$ mice were fed with regular diet. As iron-deficient mice, age-matched wild-type mice were fed with an iron-deficient diet for 4 weeks.
(F) UIBC, TIBC, and transferrin saturation in *Reg1*$^{-/-}$ mice (n = 3–4).
(G) Erythropoietin mRNA expression levels in *Reg1*$^{-/-}$ kidney (n = 8).
(H) Erythroferrone mRNA expression levels in the bone marrow cells and spleen of *Reg1*$^{-/-}$ mice (n = 6–7).
Each symbol represents the value from individual mice. Horizontal lines indicate the mean (B, C, and F). Data are expressed as mean ± SD (A, E, G, and H). Data were pooled from 13 (A), 3 (C and G), 2 (F), or 4 (H) independent experiments. *$p < 0.05$, **$p < 0.01$, ***$p < 0.001$ by Student's t test compared to *Reg1*$^{-/-}$ mice at 3 weeks of age (A) or control (B, C, and F–H) or by one-way-ANOVA with Bonferroni correction (E). #$p < 0.05$, ##$p < 0.01$, ###$p < 0.001$ (Student's t test) compared to control (A).
See also Figures S2 and S3.

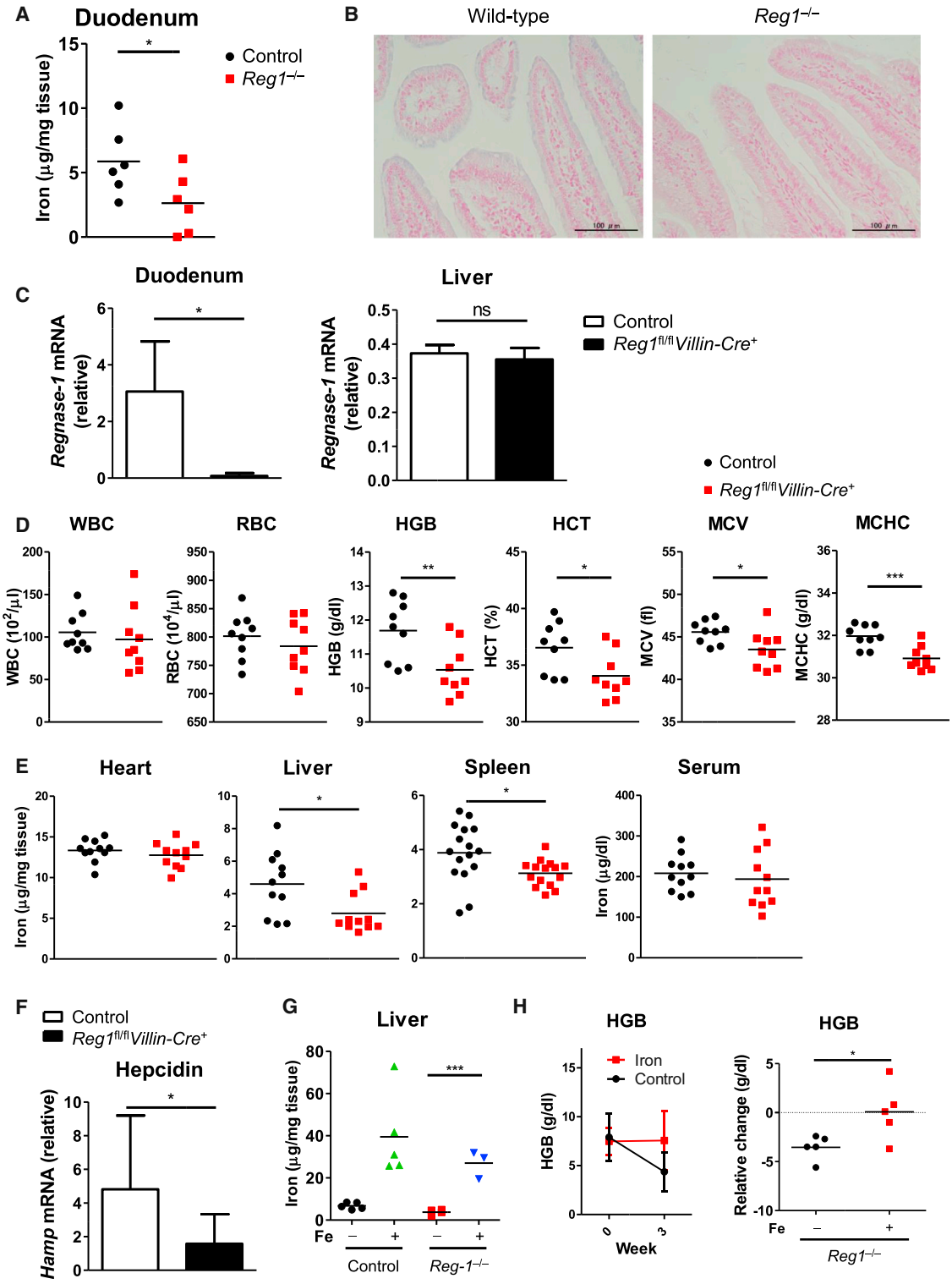


**Figure 4. Reg1 Is Required for Duodenal Iron Uptake**

(A) Iron levels of the duodenums from *Reg1*$^{-/-}$ mice (n = 6).

(B) Berlin blue stain of the duodenum. Representative images of each genotype are shown.

(C) *Reg1* mRNA expression levels in the duodenal epithelial cells and liver of *Reg1*$^{fl/fl}$*Villin-Cre*$^{+}$ mice (n = 5).

(D) Hematological parameters of *Reg1*$^{fl/fl}$*Villin-Cre*$^{+}$ mice at the age of 4–6 weeks. (n = 9). WBC, white blood cell.

*(legend continued on next page)*

the possibility that the pathogenic mechanisms of iron deficiency anemia in *Reg1*$^{-/-}$ mice are associated with ferritin upregulation in the duodenum.

## Reg1 Controls Duodenal Iron Uptake via the PHD3-HIF2α Axis

To identify Reg1 target genes regulating iron uptake, we conducted transcriptome analysis in wild-type and *Reg1*$^{-/-}$ duodenum and compared mRNA expression levels (Figure 5A). Gene ontology (GO) analysis revealed that a large number of upregulated genes in *Reg1*$^{-/-}$ duodenum were related to immune regulation or response (Table S2; Figures S6A and S6C). To focus on the iron-related targets of Reg1, we excluded genes whose GO was associated with immune regulation or response or those without a GO annotation, and we explored candidate genes regulating iron homeostasis (Figure S6B). Of non-immune related genes, top-ranked upregulated genes in *Reg1*$^{-/-}$ duodenum were sorted by multiple-testing-adjusted p value (Figure 5B; Table S2; Supplemental Experimental Procedures). Among the top-ranked genes shown in Figure 5B, *Egln3* was one of the most highly expressed genes in *Reg1*$^{-/-}$ duodenum ($p = 6.15 \times 10^{-8}$). In addition to *Egln3*, we found another potential target of duodenal Reg1, *Hif3a*, as an iron-related gene, although these genes are not depicted in Figure 5B ($p = 5.08 \times 10^{-3}$). The augmented expression of these genes was validated by qRT-PCR analysis (Figures 5C and S6D). Since the p value of *Egln3* in the *Reg1*$^{-/-}$ duodenum is substantially lower than that of *Hif3a*, we next set out to analyze the role of *Egln3* (PHD3). To date, four prolyl hydroxylases (PHD1–4, *Egln1-4*) for HIF have been identified, and PHD1–3 are thought to be crucial for inhibiting HIF activity (Kaelin and Ratcliffe, 2008). qRT-PCR analysis revealed that PHD3 is the most highly upregulated gene among these three PHD family members (Figure 5C). We next examined the relative expression of each PHD family member by comparing RPKM (reads per kilobase per million mapped reads) of the transcriptome data of PHD family members, since redundancy has been reported in controlling HIF activity (Taniguchi et al., 2014). Whereas *PHD1* (*Egln2*) and *PHD3* mRNAs were expressed in wild-type duodenum, *PHD3* mRNA was highly elevated and dominantly expressed under Reg1 deficiency (Figure 5D). In contrast, expression of *PHD1* mRNA was most abundant in both wild-type and *Reg1*$^{-/-}$ liver (Figure 5D). This difference in the relative contribution of each family member may account for the tissue-specific regulation of HIF activity by Reg1. Moreover, PHD3 expression was highly augmented in *Reg1*$^{-/-}$ duodenum compared to control at the protein level (Figure 5E).

To investigate whether *PHD3* mRNA is destabilized by Reg1, we next inserted the full-length 3′ UTR of mouse *PHD3* mRNA into a pGL3 construct and assessed luciferase activity under conditions of Reg1 overexpression. Indeed, the addition of full-length 3′ UTR of *PHD3* mRNA reduced the luciferase activity in the presence of wild-type Reg1, but not Reg1-D141N (Figure 5F). By expressing reporter constructs harboring four distinct regions of *PHD3* 3′ UTR, we found that mPHD3-3′ UTR-(801–1,230) is responsive to wild-type Reg1, while (1–430), (401–830), and (1,201–1,643) are not (Figure S6E). A putative stem-loop structure with a pyrimidine-purine-pyrimidine loop sequence (912–935) (Figure S6F) was discovered in the *PHD3* 3′ UTR (801–1,230) sequence, whose addition in the reporter gene conferred Reg1 responsiveness (Figure S6G). To further confirm that *PHD3* mRNA destabilization is accelerated by Reg1, we assessed the mRNA decay assay using the Tet-Off system. Indeed, the decay rate of *PHD3* mRNA was accelerated under the overexpression of Reg1 (Figure 5G). To test whether Reg1 is associated with *PHD3* mRNA, we next performed RIP-qPCR analysis. We found that *PHD3* mRNA, but not 18S rRNA, co-precipitated with Reg1-D141N (Figure 5H), indicating that Reg1 directly recognizes *PHD3* mRNA. These findings demonstrate that *PHD3* mRNA is a ribonucleaolytic target of Reg1.

HIF2α regulates iron homeostasis through the induction of Dmt1, Dcytb, and Fpn1 in the duodenum upon iron deficiency (Shah et al., 2009; Taylor et al., 2011). To test whether these targets are upregulated in *Reg1*$^{-/-}$ duodenum, we compared the duodenums from control and *Reg1*$^{-/-}$ mice fed with a normal diet and iron-deficient wild-type mice fed with a low-iron diet (ID mice) as a positive control of HIF2α activation. To obtain iron-deficient mice, wild-type mice were fed with a low-iron diet for 4 weeks, which was sufficient to induce iron deficiency anemia similar to that observed in *Reg1*$^{-/-}$ mice (Figure 6A). Compared to the duodenum of these iron-deficient mice, mRNA expression levels of HIF2α targets, including *Dmt1*, *Dcytb*, *Fpn1*, and *Slc38a1*, were significantly lower in *Reg1*$^{-/-}$ duodenum (Figure 6B). These findings suggest that HIF2α is not activated in *Reg1*$^{-/-}$ duodenum, even though these mice developed severe iron deficiency and anemia. Notably, mRNA levels of *TfR1*, which is presumably a HIF2α-inducible gene, were significantly higher in *Reg1*$^{-/-}$ duodenum than controls (Figure 6B), suggesting that *TfR1* mRNA is also targeted by Reg1 in the duodenum. We next examined Fpn1 expression at the protein level and confirmed that Fpn1 expression was not upregulated in *Reg1*$^{-/-}$ duodenum (Figure 6C). In line with these observations, we also found that ferric reductase activity, which determines the activity of Dcytb, was impaired in *Reg1*$^{-/-}$ duodenum compared to that of iron-deficient mice (Figure 6D). These findings indicate that HIF2α activity is impaired in *Reg1*$^{-/-}$ duodenum.

Next, to test whether the inhibition of PHD3 activity ameliorates iron deficiency in *Reg1*$^{-/-}$ mice, we utilized a HIF hydroxylase inhibitor, DMOG. Serial intraperitoneal administration of

(E) Iron levels of each organ and serum from *Reg1*$^{fl/fl}$*Villin-Cre*$^{+}$ mice at the age of 4–6 weeks (n = 11).
(F) Hepcidin mRNA expression levels in the liver of *Reg1* $^{fl/fl}$*Villin-Cre*$^{+}$ mice (n = 11).
(G) Liver iron levels of *Reg1*$^{-/-}$ mice treated with saline or iron (n = 3–5).
(H) Relative change in HGB levels of *Reg1*$^{-/-}$ mice before and after the serial iron administration (n = 5).
Each symbol represents the value from individual mice. Horizontal lines indicate the mean (A, D, E, G, and H). Data are expressed as mean ± SD (C, F, and H). Data were pooled from three (A, D, and F) or four (E) independent experiments. *p < 0.05, **p < 0.01, ***p < 0.001 by Student's t test (A, C–F, and H) or one-way ANOVA with Bonferroni correction (G). ns, not significant. See also Figures S4 and S5.

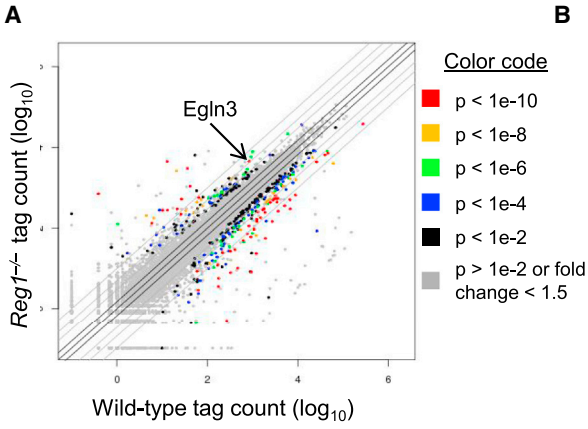


B

| Gene symbol | Wild-type RPKM | *Reg1*$^{-/-}$ RPKM | Adjusted p value |
|---|---|---|---|
| Slc5a8 | 0.0 | 10.5 | 1.4E-41 |
| Gm10104 | 1.7 | 53.3 | 4.5E-17 |
| Ceacam10 | 1.7 | 39.1 | 1.2E-16 |
| Ak4 | 0.3 | 4.6 | 1.6E-15 |
| Scn8a | 0.1 | 1.9 | 1.7E-15 |
| 1600029D21Rik | 1.3 | 128.6 | 1.3E-12 |
| 2310014F07Rik | 1.9 | 166.1 | 1.2E-09 |
| Hemt1 | 0.5 | 17.4 | 8.5E-09 |
| Gml | 0.3 | 18.0 | 1.5E-08 |
| Nkain1 | 1.9 | 15.6 | 2.0E-08 |
| Egln3 | 21.4 | 131.8 | 6.2E-08 |
| Gm15299 | 0.2 | 35.2 | 1.5E-07 |
| Fpr2 | 0.1 | 1.4 | 2.2E-06 |
| Clec4a3 | 0.4 | 4.0 | 8.8E-06 |
| Unc5cl | 18.2 | 80.1 | 1.6E-05 |

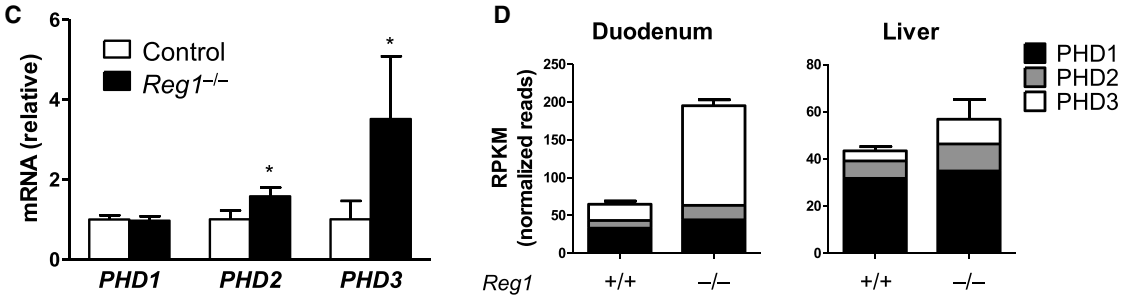


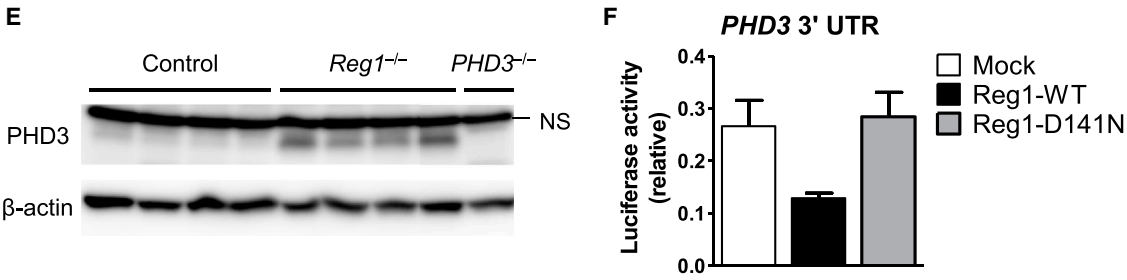


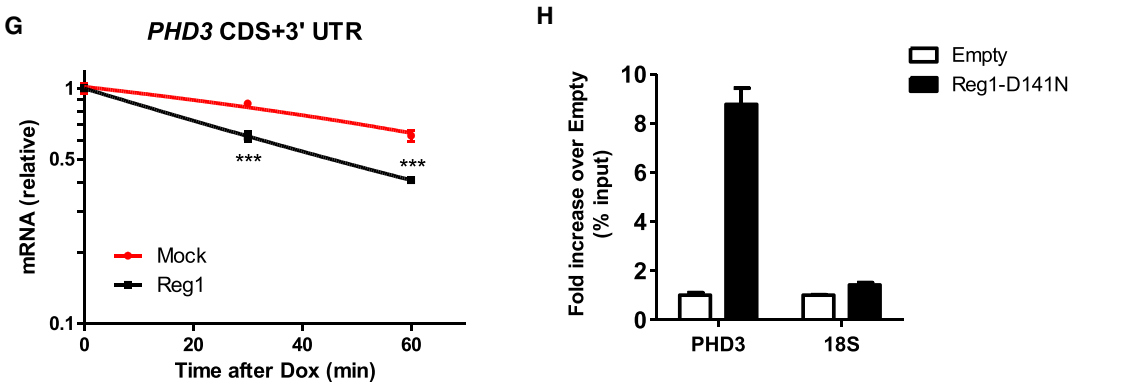


**Figure 5. Identification of the Reg1 Target Responsible for Iron Deficiency**

(A) Scatterplot comparing transcriptome of the duodenum from wild-type and *Reg1*$^{-/-}$ mice (n = 2). See also Table S2.

(B) Top-ranked GO-annotated genes unrelated to immune regulation or response.

(C) *PHD1-3* mRNA expression levels in *Reg1*$^{-/-}$ duodenum (n = 4–5).

*(legend continued on next page)*

DMOG increased mRNA levels of HIF2α-inducible genes in *Reg1*$^{-/-}$ duodenum, suggesting that this treatment, at least to some extent, reversed the HIF2α activity in *Reg1*$^{-/-}$ duodenum (Figure S5D). After treatment with DMOG, tissue iron levels in the liver increased in *Reg1*$^{-/-}$ mice, while this treatment did not alter tissue iron levels in age-matched wild-type mice (Figures 6E and S5E). Furthermore, we asked whether genetic ablation of PHD3 ameliorated anemia and iron deficiency in *Reg1*$^{-/-}$ mice by utilizing mice deficient in both Reg1 and PHD3 (*PHD3*$^{-/-}$*Reg1*$^{-/-}$ mice). We found that HGB levels, MCV, and splenic tissue iron levels were significantly elevated in *PHD3*$^{-/-}$*Reg1*$^{-/-}$ mice compared to *Reg1*$^{-/-}$ mice (Figures 6F and 6G). Collectively, these findings suggest that Reg1 destabilizes *PHD3* mRNA to facilitate duodenal iron uptake.

### Reg1 Is Transcriptionally Upregulated by Iron Deficiency via an HRE in Its Promoter

Next, we asked whether Reg1 expression itself is regulated by iron concentrations. To address this question, we assessed mRNA levels of Reg1 in the duodenum of iron-deficient mice. Interestingly, *Reg1* mRNA expression in the duodenum was significantly higher in iron-deficient mice than in control mice (Figure 7A). This finding suggests Reg1 expression in the duodenum is regulated in an iron-mediated manner.

Mouse Reg1 harbors two putative HREs in its promoter region in the vicinity of the translation start site (TSS) (HRE1 and HRE2; Figure 7B; Supplemental Experimental Procedures). Therefore, we next asked whether Reg1 expression is inducible via the activity of HIF1α and/or HIF2α. To test this idea, we made a luciferase reporter vector containing the mouse Reg1 promoter region (−500-TSS), where two putative HREs are located (Figure 7C), and conducted a luciferase assay. The overexpression of constitutively active HIF2α, but not HIF1α, increased luciferase activity (Figure 7D), suggesting that the Reg1 promoter region is specifically responsive to HIF2α. Furthermore, the reporter harboring HRE1 responded to constitutive-active HIF2α, but not the one lacking HRE1, suggesting that HRE1, but not HRE2, in the murine Reg1 promoter region is the functional HRE (Figures 7C and 7D). Collectively, these findings support a model where Reg1 is inducible upon iron deficiency via the HIF2α-responsive HRE.

To test whether the physiological changes in Reg1 expression during iron deficiency impact iron homeostasis, we next utilized the Reg1 hypomorphic strain of mouse, which was fortuitously obtained by the addition of FLAG at the 5′ end of the Reg1 coding sequence (Figures S7A and S7B). In the duodenal epithelial cells of these hypomorphic mice, Reg1 expression levels decreased to 30% of those of control mice (Figure S7C). While hypomorphic mice did not show any signs of inflammation, unlike *Reg1*$^{-/-}$ mice (data not shown), they suffered from microcytic anemia and iron deficiency at the age of 3–4 weeks (Figures S7D and S7E). These findings suggest that the physiological changes in Reg1 expression, observed under iron-deficient conditions, control iron homeostasis.

To further analyze the physiological role of the regulation of Reg1 expression in iron metabolism, we utilized the model of chronic iron deficiency induced by a low-iron diet, in which Reg1 expression is induced (Figure 7A). In this model, anemia was more severe in *Reg1*$^{fl/fl}$*Villin-Cre*$^{+}$ mice than in control mice at all time points with the low-iron diet (Figure 7E). Also, anemia progressed more rapidly in *Reg1*$^{fl/fl}$*Villin-Cre*$^{+}$ mice (Figure 7F). These findings support a model where induction of Reg1 in duodenal epithelial cells facilitates iron uptake during iron deficiency.

## DISCUSSION

In the current study, we revealed that Reg1 serves as a critical regulator in iron homeostasis. This conclusion is based on the following findings: (1) Reg1 destabilized a set of mRNAs relating to iron homeostasis, including *TfR1* and *PHD3*; (2) *Reg1*$^{-/-}$ mice suffered from severe iron deficiency anemia, which was largely independent of inflammation and hepcidin; (3) inhibition of PHD3 activity ameliorated the defect in duodenal iron uptake found in *Reg1*$^{-/-}$ mice; and (4) Reg1 expression was inducible upon iron deficiency via HIF2α. These findings established a working model for Reg1-mediated regulation of duodenal iron absorption (Figure S7F). Upon iron deficiency, accumulated HIF2α transactivates Reg1 via the HRE in the Reg1 promoter. Reg1 protein then promotes mRNA decay of PHD3, leading to further stabilization of HIF2α. Thus, Reg1 forms a positive feedback mechanism for HIF2α activation in the duodenum.

Although it was proposed that *TfR1* mRNA undergoes endonucleolytic degradation via its 3′ UTR, endogenous endonucleases for *TfR1* mRNA decay have long remained unidentified (Binder et al., 1994). In this study, we identified Reg1 as a nuclease responsible for endonucleolytic cleavage of *TfR1* mRNA. We found that the 3′ UTR of *TfR1* mRNA contains a Reg1-responsive sequence that is predicted to form a stem-loop structure. Distinct from that of IREs, the loop pattern in the stem-loop structure found in *TfR1* mRNA is pyrimidine-purine-pyrimidine, consistent with our findings from a genome-wide analysis of Reg1 targets (Mino et al., 2015). This view is also supported by a previous study, which demonstrated the

(D) mRNA expression levels (RPKM) of PHD genes in the duodenum and liver of wild-type and *Reg1*$^{-/-}$ mice (n = 2).
(E) Immunoblot analysis of PHD3 and β-actin in the duodenal epithelial cells from *Reg1*$^{-/-}$ mice (n = 4). NS, non-specific band.
(F) HEK293T cells were co-transfected with pGL3-mPHD3-3′ UTR and the expression plasmids for Reg1-WT, Reg1-D141N, or mock. After 48 hr of incubation, the luciferase activity of cell lysates was determined.
(G) HEK293 Tet-Off cells were co-transfected with pTREtight-mPHD3-CDS-3′ UTR, together with the Reg1 expression vector or the control (mock). Total RNAs were extracted after Dox (1 μg/mL) treatment, and levels of *PHD3* mRNA were measured by qRT-PCR.
(H) HEK293T cells were transfected with Reg1-D141N expression vector or the control (empty). RNA-protein complexes were immunoprecipitated, and levels of *PHD3* mRNA and 18S rRNA were measured by qRT-PCR.
Data are expressed as mean ± SD of biological replicates (C and D) or triplicates (F–H). *$p < 0.05$, ***$p < 0.001$ (Student's t test; C and G). Data are representative of three (F and G) or two (H) independent experiments. See also Figure S6 and Table S2.

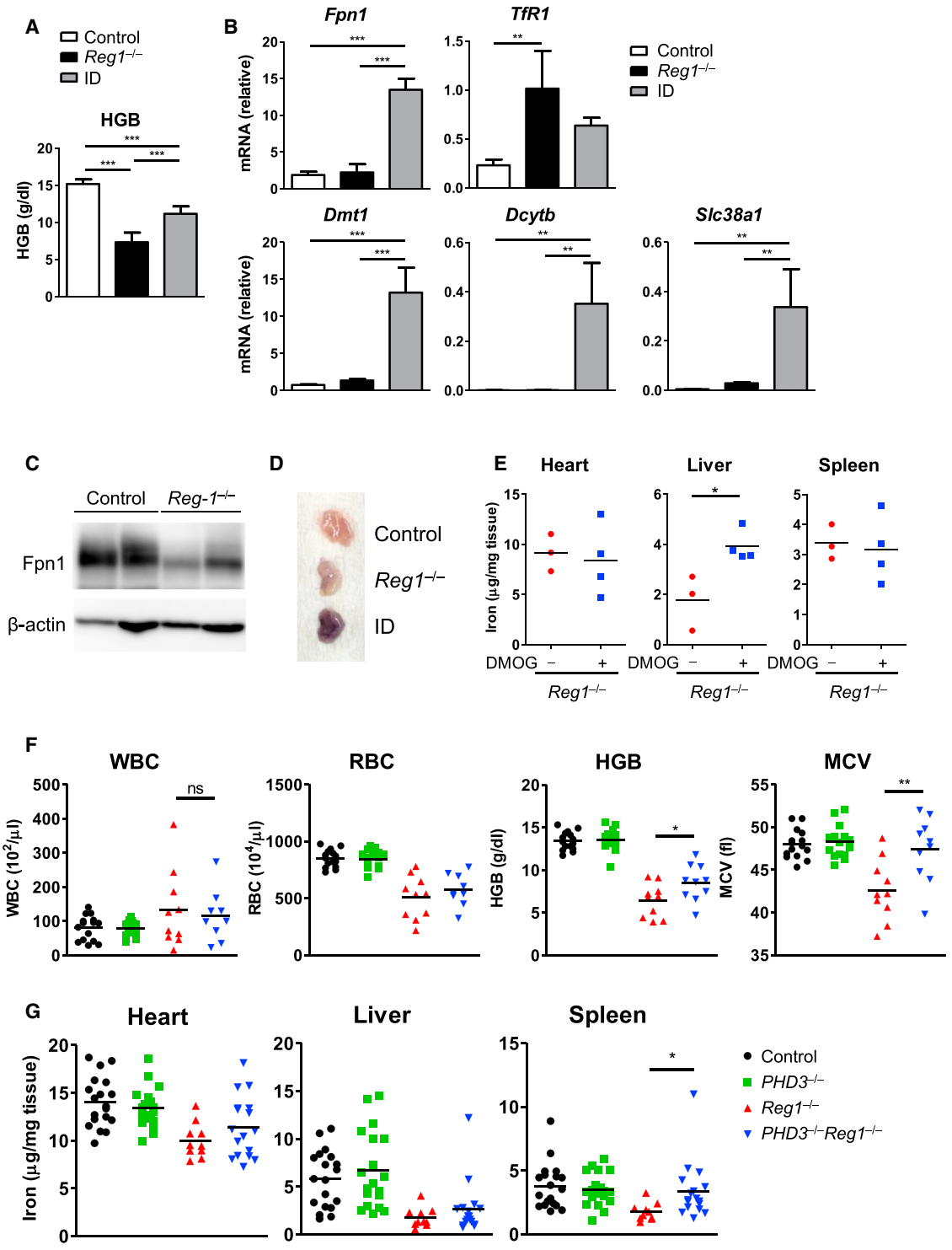


**Figure 6. Reg1 Regulates Duodenal Iron Uptake by Controlling PHD3 Expression**

(A and B) Control and *Reg1*$^{-/-}$ mice were fed a regular diet. Iron-deficient mice (ID; age-matched wild-type mice) were fed a low-iron diet for 4 weeks. (A) HGB levels of control, *Reg1*$^{-/-}$ and ID mice. (B) mRNA expression levels of HIF2α target genes in control, *Reg1*$^{-/-}$ and ID duodenum (n = 4–5).

(C) Immunoblot analysis of ferroportin (Fpn1) and β-actin in the duodenal epithelial cells from *Reg1*$^{-/-}$ mice (n = 2).

(D) Ferric reductase assay in control and *Reg1*$^{-/-}$ duodenum. Increased activity of ferric reductase was detected as purple staining. The image is representative of two independent experiments.

(E) Tissue iron levels of *Reg1*$^{-/-}$ mice treated with DMOG or saline for 2 weeks (n = 3–4).

*(legend continued on next page)*

region adjacent to this putative stem-loop structure (the region between 76 and 90 in the TRS-1 3′ UTR, which is a fragment of human *TfR1* mRNA utilized to determine the endonucleolytic cleavage site) is the cleavage site by unknown endonucleases (the region between 185 and 186 in the TRS-1 3′ UTR) (Binder et al., 1994) (Figure S1C). Although the biological role of *TfR1* mRNA decay needs further clarification, it is clear that Reg1 serves as an endogenous endonuclease for the mRNAs of iron-controlling genes, including *TfR1* mRNA.

Multiple RNA-binding proteins are engaged in mRNA stabilization or decay (Kafasla et al., 2014). For example, we have shown that the RNA-binding proteins Reg1 and Roquin-1/2 target a common set of mRNAs to ensure the cessation of gene expression, although the temporal and spatial regulation of mRNA decay is distinct (Mino et al., 2015). *TfR1* mRNA harbors five IREs in its 3′ UTR, which increases mRNA stability via IRPs. On the other hand, we identified an evolutionarily conserved stem-loop structure in *TfR1* mRNA, which is recognized by Reg1. We further showed that Reg1 has the potential to cancel *TfR1* mRNA stabilization by IRPs, suggesting the model of steric competition between IRPs and Reg1 binding. These findings imply that Reg1 participates in elaborate regulatory mechanisms that control the stability of *TfR1* mRNA.

It has been reported that another RNA-binding protein, TTP, which promotes the deadenylation of ARE-containing mRNAs, negatively regulates *TfR1* mRNA (Bayeva et al., 2012). However, it has also been suggested that endonucleolytic cleavage, but not deadenylation, was involved in the decay of 3′ UTR of *TfR1* mRNA under specific experimental conditions (Binder et al., 1994). Here, we have shown that Reg1 destabilizes *TfR1* mRNA through the recognition of an evolutionarily conserved stem-loop structure, providing a likely identity of the previously "unknown endonuclease" for *TfR1* mRNA. It would be intriguing in the future to clarify the relationship between endo- and exonucleolytic degradation in controlling *TfR1* mRNA.

It is widely viewed that hepcidin is a key regulator in anemia of inflammation (Ganz and Nemeth, 2015; Weiss and Goodnough, 2005). We have previously shown that Reg1 suppresses the expression of IL-6, which is a strong inducer of hepcidin (Matsushita et al., 2009). Nevertheless, we have found that hepcidin levels are highly suppressed in *Reg1*$^{-/-}$ mice despite severe autoimmune inflammation. Hepcidin mRNA levels in the liver, which is the main source of serum hepcidin, were virtually undetectable in *Reg1*$^{-/-}$ mice. These findings clearly indicate that anemia in *Reg1*$^{-/-}$ mice is not caused by hepcidin upregulation. It is plausible that hepcidin suppression is caused by severe iron deficiency in the liver, since iron supplementation, at least to some extent, upregulated hepcidin mRNA expression. Also, erythroferrone upregulation produced by erythroblasts contributes to the suppression of hepcidin in *Reg1*$^{-/-}$ mice. Taken together, the anemia and iron deficiency observed in *Reg1*$^{-/-}$ mice are not typical of the anemia of inflammation, which is largely dependent on hepcidin-mediated suppression of Fpn1. Furthermore, we have found that Reg1 plays an essential role in iron uptake through the destabilization of *PHD3* mRNA and that its expression is inducible upon iron deficiency via HIF2α. Thus, while suppression of the systemic iron hormone hepcidin promotes duodenal iron export via stabilization of Fpn1, Reg1 may serve as a local facilitator of iron uptake in the duodenum via the PHD3-HIF2α axis under conditions of iron deficiency.

The role of Reg1 in controlling iron homeostasis is largely distinct from its role in the regulation of inflammation. First, we demonstrated that mice deficient in both Reg1 and Rag2, in which mature lymphocytes and immunoglobulins are absent, totally recapitulated the features of anemia found in *Reg1*$^{-/-}$ mice. Second, we failed to find gastritis in *Reg1*$^{-/-}$ mice despite extensive histological examination, as reported previously (Zhou et al., 2013). Third, mice lacking Reg1 in intestinal epithelial cells alone had iron deficiency anemia without any obvious evidence of inflammation. Whereas a previous report suggested that *Reg1*$^{-/-}$ mice develop anemia because of autoimmunity to RBCs and parietal cells (Zhou et al., 2013), the findings above, particularly the fact that antibodies are not necessary in the development of anemia under Reg1 deficiency, failed to support this observation. Although the contribution of autoimmune disease to altered iron homeostasis in *Reg1*$^{-/-}$ mice needs further clarification, this study clearly demonstrates that mechanisms independent of autoimmune disease are sufficient to induce iron deficiency anemia in *Reg1*$^{-/-}$ mice.

Mice that lack Reg1 only in intestinal epithelial cells developed iron deficiency anemia, although the phenotype was milder compared to *Reg1*$^{-/-}$ mice. This difference may result from the incomplete deletion of Reg1 in the target organ due to the limitations of the Cre-*loxP* system. Since duodenal epithelial cells have the capacity to adaptively increase iron uptake by ~20-fold during periods of iron deficiency (Carpenter and Ummadi, 1995), the remaining activity of Reg1 in a small portion of cells may compensate for the decline in iron uptake. Indeed, a percentage of duodenal epithelial cells in *Reg1*$^{fl/fl}$*Villin-Cre*$^{+}$ mice harbor intact Reg1 (Figure 4C). This view is supported by the observation that a low-iron diet exacerbates the phenotype of mice lacking Reg1 in intestinal epithelial cells. It is of note that these phenotypes of *Reg1*$^{fl/fl}$*Villin-Cre*$^{+}$ mice mentioned above were reminiscent of those of the mice that lack HIF2α in intestinal epithelial cells (Taylor et al., 2011). Taylor et al. (2011) reported that *HIF2α*$^{fl/fl}$*Villin-Cre*$^{+}$ mice show severe anemia only after treatment with a low-iron diet. This similarity in phenotype implies a mechanistic overlap of Reg1 and HIF2α.

Iron homeostasis is tightly controlled during inflammatory responses. We have previously shown that the expression of Reg1 is controlled by a variety of inflammatory stimuli. Reg1 was shown to be a lipopolysaccharide (LPS)-inducible gene in PECs (Matsushita et al., 2009). In response to signaling through the IL-1 receptor or Toll-like receptors, Reg1 is ubiquitinated and

(F) Hematological parameters of control, *PHD3*$^{-/-}$, *Reg1*$^{-/-}$ and *PHD3*$^{-/-}$*Reg1*$^{-/-}$ mice (n = 9–15).
(G) Iron levels of each organ from 5-6-week-old control, *PHD3*$^{-/-}$, *Reg1*$^{-/-}$ and *PHD3*$^{-/-}$*Reg1*$^{-/-}$ mice (n = 10–19).
Each symbol represents the value from individual mice and horizontal lines indicate the mean (E–G). Data were pooled from 2 (E), 11 (F), or 12 (G) independent experiments. Data are expressed as mean ± SD of biological replicates (A and B). *p < 0.05, **p < 0.01, ***p < 0.001 by Student's t test (E–G) or one-way ANOVA with Bonferroni correction (A and B). See also Figure S5.

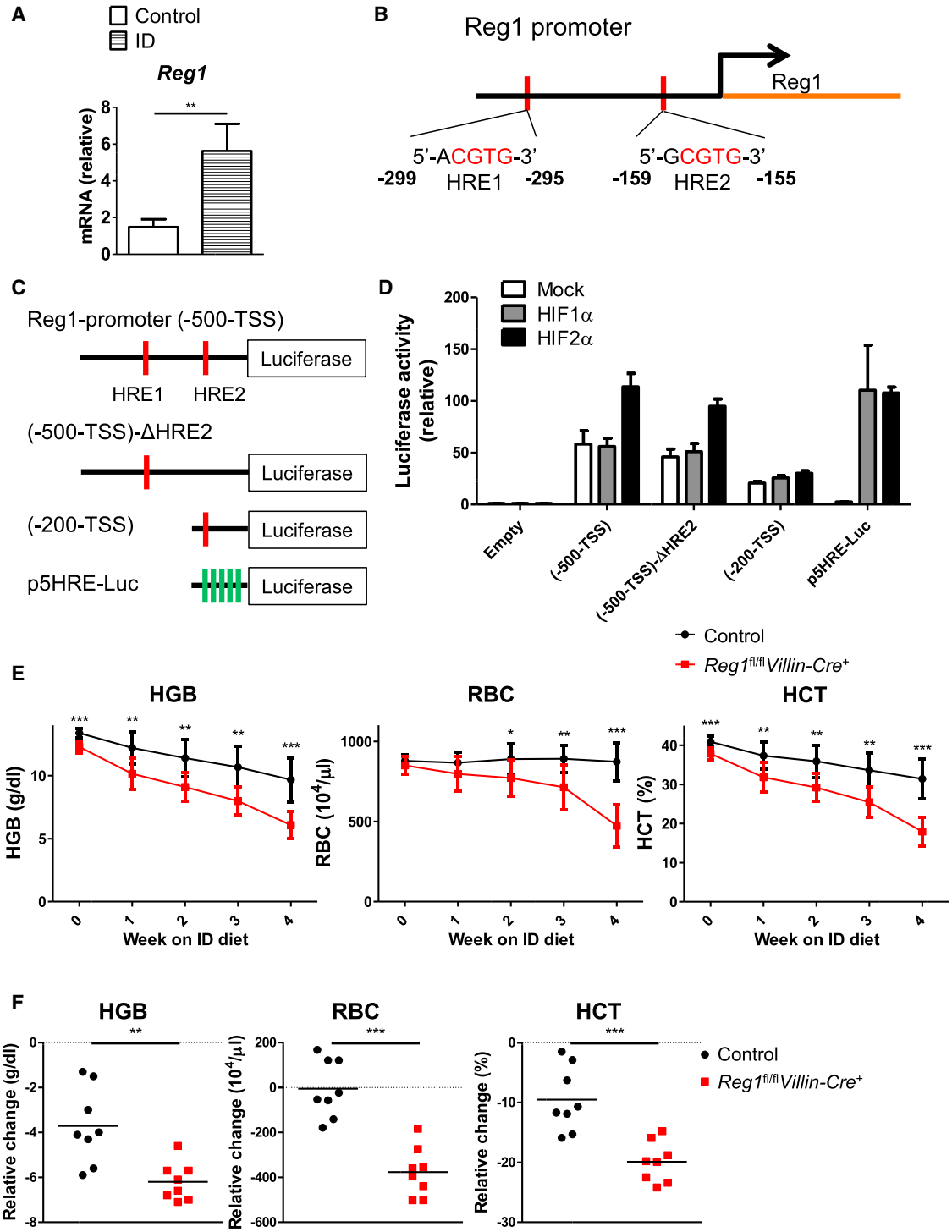


**Figure 7. HIF2α Transcriptionally Upregulates Reg1 to Activate a Positive Feedback Loop**

(A) *Reg1* mRNA expression levels in control and ID duodenums (n = 4–5).

(B) Schematic representation of two putative HRE sites in the murine Reg1 promoter region.

(C and D) HCT116 cells were co-transfected with a series of luciferase reporter plasmids (C), together with the expression plasmids for constitutive-active mutant HIF1α or HIF2α, or empty plasmid as a control (mock). After 24 hr of incubation, luciferase activity of cell lysates was determined (D). Data are representative of three independent experiments.

*(legend continued on next page)*

then degraded (Iwasaki et al., 2011). Also, T cell receptor stimulation leads to the cleavage of Reg1 by Malt1/paracaspase (Uehata et al., 2013). In addition, we showed that the transcription of Reg1 is also responsive to HIF2α. These elaborate transcriptional and post-transcriptional regulations of Reg1 expression may facilitate crosstalk between inflammation and iron homeostasis.

We identified *PHD3* mRNA as a target of Reg1 for degradation. Previous studies revealed that PHD family members function redundantly or non-redundantly depending on experimental settings and tissues. It has been reported that PHD family members play an overlapping role in protecting from radiation-induced gastrointestinal toxicity in the large and small intestine (Taniguchi et al., 2014). However, in the intestine, the duodenum is the main site of dietary iron uptake, and the role of each PHD family member in the regulation of HIF2α might not be the same. Indeed, we found that *PHD3* mRNA was the dominant transcripts among PHD family members in the duodenum lacking Reg1, supporting the notion that PHD3 is an important regulator of iron homeostasis in the duodenum. Also, we have shown that Reg1-mediated decay of *PHD3* mRNA is critical for promoting iron uptake in the duodenum. Moreover, several other studies have suggested that PHD3 has a specific role in destabilizing HIF2α and is subjected to differential regulation (Appelhoff et al., 2004; Taniguchi et al., 2013; Walmsley et al., 2011). Collectively, these findings support the notion that PHD3 in the duodenum has a non-redundant role and is subjected to differential regulation.

We have shown that Reg1-mediated decay of *PHD3* mRNA participates in a positive feedback loop that amplifies the activity of HIF2α. When this loop was disrupted by lack of Reg1 in intestinal epithelial cells, the anemia induced by a low-iron diet was exacerbated more rapidly in vivo. These findings suggest that Reg1-mediated positive feedback expression of HIF2α is critical for efficient duodenal iron uptake under conditions of iron deficiency. Interestingly, another hypoxia-inducible factor, HIF1α, is known to be amplified via PHD3 and PKM2 (Luo et al., 2011; Palsson-McDermott et al., 2015). Also it has been reported that, upon hypoxia, a HIF-inducible microRNA activates HIF1α by decreasing levels of glycerol-3-phosphate dehydrogenase 1-like (GPD1L) (Kelly et al., 2011). Thus, positive feedback could be a common regulatory mechanism for HIF activation.

Lack of PHD3 in Reg1-deficient mice significantly improved iron deficiency anemia observed in Reg1 single-knockout mice. However, the effect of PHD3 ablation in fully restoring iron levels is not perfect, suggesting that Reg1 has additional target mRNAs for controlling iron uptake. Indeed, a search of genes upregulated in *Reg1*$^{-/-}$ duodenum identified HIF3α as a potential target of Regnase-1, though the difference in expression between wild-type and *Reg1*$^{-/-}$ duodenum was markedly less significant compared to PHD3 ($p = 5.08 \times 10^{-3}$ versus $p = 6.15 \times 10^{-8}$) (Table S2). HIF3α has been implicated in the inhibition of HIF1/2α and potentially contributes to impaired HIF2α activation under Reg1 deficiency, though its function might be different depending on splice variants, and its role in iron metabolism is not known. Although it is plausible that Reg1 controls duodenal iron uptake via HIF3α and other modestly regulated target genes in addition to PHD3, further studies are needed to fully uncover the mechanisms of iron uptake regulation.

In conclusion, we have clearly shown that Reg1 is critical for mRNA destabilization of iron-controlling genes and facilitation of duodenal iron uptake by acting as the amplifier of HIF2α activation. Our results will provide insight into the regulation of iron-regulating transcripts via RNA-binding proteins.

## EXPERIMENTAL PROCEDURES

### Mice

*Regnase-1*$^{-/-}$ (*Reg1*$^{-/-}$), *Reg1*$^{fl/fl}$, *Rag2*$^{-/-}$, *PHD3*$^{-/-}$, and *Villin-Cre* transgenic mice have been described previously (el Marjou et al., 2004; Matsushita et al., 2009; Shinkai et al., 1992; Takeda et al., 2006; Uehata et al., 2013). Hypomorphic FLAG-Reg1 mice were generated as described in Supplemental Experimental Procedures. Male and female animals were used between 3 and 9 weeks of age. All animal experiments were conducted in compliance with the regulations approved by the Committee for Animal Experiments of the Institute for Frontier Life and Medical Sciences, Kyoto University. Please see Supplemental Experimental Procedures for details regarding animal experiments.

### Tissue Harvest

Please see Supplemental Experimental Procedures for details.

### Flow Cytometric Analysis

Flow cytometric analysis was performed as described previously (Matsushita et al., 2009) and in Supplemental Experimental Procedures.

### Isolation of Duodenal Epithelial Cells

Duodenal epithelial cells were isolated as described previously (Nowarski et al., 2015) and in Supplemental Experimental Procedures.

### Immunoblot Analysis

Please see Supplemental Experimental Procedures for a list of antibodies used in this study and detailed procedures. Chemiluminescent detection was performed using ImageQuant LAS 4000 or Amersham Imager 600 (GE Healthcare). Densitometric analysis was performed using NIH ImageJ software.

### qPCR Analysis

Please see Supplemental Experimental Procedures for detailed procedures and primers used in this study.

### RNA Sequencing and Bioinformatics Analysis

Proximal duodenums were immersed in TRIzol (Invitrogen) and immediately homogenized. Total RNA was then extracted according to the manufacturer's instructions. Transcriptome data were collected as described previously (Uehata et al., 2013). The method DESeq was utilized to estimate significant differentially expressed genes between wild-type and Reg1-deficient duodenums (duplicate samples).

HREs were predicted in the Reg1 promoter by scanning them with the corresponding position weight matrix (PWM) from the Jaspar database (matrix ID: MA0259.1). A PWM threshold score was set in a way that results in approximately one predicted binding site per 5 kb of the mouse genome (mm10). Scanning of the region −500 to −1 relative to the Reg1 TSS resulted in two significant hits for the HRE.

(E and F) *Reg1*$^{fl/fl}$*Villin-Cre*$^{+}$ and control mice were fed a low-iron diet for 4 weeks (n = 8). Hematological parameters were determined at the indicated time points (E). The relative change in hematological parameters before (week 0) and after (week 4) the induction of iron deficiency (F) is shown.
Each symbol represents the value from individual mice, and horizontal lines indicate the mean (F). Data are expressed as mean ± SD of biological replicates (A and E) or of triplicates (D). *$p < 0.05$, **$p < 0.01$, ***$p < 0.001$ (Student's t test) compared to control (A, E, and F). See also Figure S7.

### Analysis of Microarray Datasets

Microarray datasets (GEO: GSE14891) have been described previously (Matsushita et al., 2009). These datasets were analyzed as described in Supplemental Experimental Procedures.

### Hematological Analysis

Hematological analysis was performed using Celltac $\alpha$ hematology analyzers (MEK 6450, Nihon Kohden).

### Tissue and Serum Iron Quantification

Tissue and serum iron quantification was conducted using a metalloassay kit (ferrozine method) according to the manufacturer's instructions (MG Metallogenics) as described in Supplemental Experimental Procedures.

### Determination of UIBC

UIBC was determined using a microassay UIBC kit (MG Metallogenics) according to the manufacturer's instructions as described in Supplemental Experimental Procedures.

### Ferric Reductase Assay

Ferric reductase assay was performed as described previously (Shah et al., 2009) and in Supplemental Experimental Procedures.

### Histological Analysis

Tissue-iron detection was performed in formalin-fixed paraffin-embedded sections stained with Berlin blue.

### RNA Secondary Structure Prediction

The mfold program was used for RNA secondary structure predictions (Zuker, 2003).

### Luciferase Assay

Luciferase assay was performed as described previously (Matsushita et al., 2009) and in the Supplemental Experimental Procedures.

### mRNA Decay Assay

The mRNA decay assay was performed as described previously (Matsushita et al., 2009) and in Supplemental Experimental Procedures.

### RIP Assay

Please see Supplemental Experimental Procedures for details.

### Immunoprecipitation of FLAG-Reg1

Please see Supplemental Experimental Procedures for details.

### Statistical Analysis

Results are expressed as mean ± SD. Statistical analyses were performed using Prism v.5 (GraphPad). Statistical significance was calculated using a two-tailed Student's t test or one-way ANOVA with Bonferroni correction. p values of less than 0.05 were considered significant (*$p < 0.05$, **$p < 0.01$, ***$p < 0.001$, #$p < 0.05$, ##$p < 0.01$, ###$p < 0.001$).

## ACCESSION NUMBERS

The accession number for the RNA-sequencing data in Table S2 is DDBJ: DRA003215.

## SUPPLEMENTAL INFORMATION

Supplemental Information includes Supplemental Experimental Procedures, seven figures, and two tables and can be found with this article online at http://dx.doi.org/10.1016/j.celrep.2017.05.009.

## AUTHOR CONTRIBUTIONS

M.Y., T.M., and O.T. designed the experiments and analyzed the data. M.Y. performed most of the experiments. D.O., T.U., Y.N., and T.M. helped with experiments. Y.N. generated FLAG-Reg1 mice. A.V. performed the bioinformatics analysis. T.T. performed the histological analysis. Y.S. conducted the RNA sequencing and processed the data. M.Y., A.V., and O.T. wrote the manuscript. O.T. supervised the project.

## ACKNOWLEDGMENTS

We thank D.M. Standley (Osaka University) and all members of our laboratory for helpful discussion; Y. Asahira and M. Tsuji for secretarial assistance; and K. Imamura, M. Tosaka, and T. Horiuchi (Tokyo University) for technical assistance. We also thank G.H. Fong and K. Takeda (University of Connecticut), K. Hirota, T. Nakagawa, and K. Ikuta (Kyoto University) for mice and K. Iwai, E. Nakamura, H. Harada, and M. Noda (Kyoto University) for reagents. This work was supported by a grant-in-aid for Scientific Research on Innovative Areas ''Genome Science'' from the Ministry of Education, Culture, Sports, Science, and Technology of Japan (221S0002 and 16H06279; O.T. and T.M.), the Japan Society for the Promotion of Science (JSPS) Core-to-Core Program, and grants from the Takeda Science Foundation and Uehara Memorial Foundation (O.T.). M.Y. is the recipient of a Takeda Science Foundation scholarship.

Received: September 12, 2016
Revised: March 30, 2017
Accepted: May 2, 2017
Published: May 23, 2017

## REFERENCES

Appelhoff, R.J., Tian, Y.M., Raval, R.R., Turley, H., Harris, A.L., Pugh, C.W., Ratcliffe, P.J., and Gleadle, J.M. (2004). Differential function of the prolyl hydroxylases PHD1, PHD2, and PHD3 in the regulation of hypoxia-inducible factor. J. Biol. Chem. *279*, 38458–38465.

Arcus, V.L., McKenzie, J.L., Robson, J., and Cook, G.M. (2011). The PIN-domain ribonucleases and the prokaryotic VapBC toxin-antitoxin array. Protein Eng. Des. Sel. *24*, 33–40.

Bayeva, M., Khechaduri, A., Puig, S., Chang, H.C., Patial, S., Blackshear, P.J., and Ardehali, H. (2012). mTOR regulates cellular iron homeostasis through tristetraprolin. Cell Metab. *16*, 645–657.

Binder, R., Horowitz, J.A., Basilion, J.P., Koeller, D.M., Klausner, R.D., and Harford, J.B. (1994). Evidence that the pathway of transferrin receptor mRNA degradation involves an endonucleolytic cleavage within the 3′ UTR and does not involve poly(A) tail shortening. EMBO J. *13*, 1969–1980.

Carpenter, C.E., and Ummadi, M. (1995). Iron status alters the adsorption, uptake, and absorption capacities of rat duodenum for ferrous and ferric iron. Nutr. Res. *15*, 1129–1138.

Drakesmith, H., Nemeth, E., and Ganz, T. (2015). Ironing out Ferroportin. Cell Metab. *22*, 777–787.

el Marjou, F., Janssen, K.P., Chang, B.H., Li, M., Hindie, V., Chan, L., Louvard, D., Chambon, P., Metzger, D., and Robine, S. (2004). Tissue-specific and inducible Cre-mediated recombination in the gut epithelium. Genesis *39*, 186–193.

Galy, B., Ferring-Appel, D., Becker, C., Gretz, N., Gröne, H.J., Schümann, K., and Hentze, M.W. (2013). Iron regulatory proteins control a mucosal block to intestinal iron absorption. Cell Rep. *3*, 844–857.

Ganz, T., and Nemeth, E. (2015). Iron homeostasis in host defence and inflammation. Nat. Rev. Immunol. *15*, 500–510.

Iwasaki, H., Takeuchi, O., Teraguchi, S., Matsushita, K., Uehata, T., Kuniyoshi, K., Satoh, T., Saitoh, T., Matsushita, M., Standley, D.M., and Akira, S. (2011). The IκB kinase complex regulates the stability of cytokine-encoding mRNA induced by TLR-IL-1R by controlling degradation of regnase-1. Nat. Immunol. *12*, 1167–1175.

Kaelin, W.G., Jr., and Ratcliffe, P.J. (2008). Oxygen sensing by metazoans: the central role of the HIF hydroxylase pathway. Mol. Cell *30*, 393–402.

Kafasla, P., Skliris, A., and Kontoyiannis, D.L. (2014). Post-transcriptional coordination of immunological responses by RNA-binding proteins. Nat. Immunol. *15*, 492–502.

Kautz, L., Jung, G., Valore, E.V., Rivella, S., Nemeth, E., and Ganz, T. (2014). Identification of erythroferrone as an erythroid regulator of iron metabolism. Nat. Genet. *46*, 678–684.

Kelly, T.J., Souza, A.L., Clish, C.B., and Puigserver, P. (2011). A hypoxia-induced positive feedback loop promotes hypoxia-inducible factor 1alpha stability through miR-210 suppression of glycerol-3-phosphate dehydrogenase 1-like. Mol. Cell. Biol. *31*, 2696–2706.

Kühn, L.C. (2015). Iron regulatory proteins and their role in controlling iron metabolism. Metallomics *7*, 232–243.

Luo, W., Hu, H., Chang, R., Zhong, J., Knabel, M., O'Meally, R., Cole, R.N., Pandey, A., and Semenza, G.L. (2011). Pyruvate kinase M2 is a PHD3-stimulated coactivator for hypoxia-inducible factor 1. Cell *145*, 732–744.

Mastrogiannaki, M., Matak, P., Keith, B., Simon, M.C., Vaulont, S., and Peyssonnaux, C. (2009). HIF-2alpha, but not HIF-1alpha, promotes iron absorption in mice. J. Clin. Invest. *119*, 1159–1166.

Matsushita, K., Takeuchi, O., Standley, D.M., Kumagai, Y., Kawagoe, T., Miyake, T., Satoh, T., Kato, H., Tsujimura, T., Nakamura, H., and Akira, S. (2009). Zc3h12a is an RNase essential for controlling immune responses by regulating mRNA decay. Nature *458*, 1185–1190.

Mino, T., Murakawa, Y., Fukao, A., Vandenbon, A., Wessels, H.H., Ori, D., Uehata, T., Tartey, S., Akira, S., Suzuki, Y., et al. (2015). Regnase-1 and roquin regulate a common element in inflammatory mRNAs by spatiotemporally distinct mechanisms. Cell *161*, 1058–1073.

Muckenthaler, M.U., Rivella, S., Hentze, M.W., and Galy, B. (2017). A red carpet for iron metabolism. Cell *168*, 344–361.

Nowarski, R., Jackson, R., Gagliani, N., de Zoete, M.R., Palm, N.W., Bailis, W., Low, J.S., Harman, C.C., Graham, M., Elinav, E., and Flavell, R.A. (2015). Epithelial IL-18 equilibrium controls barrier function in colitis. Cell *163*, 1444–1456.

Palsson-McDermott, E.M., Curtis, A.M., Goel, G., Lauterbach, M.A., Sheedy, F.J., Gleeson, L.E., van den Bosch, M.W., Quinn, S.R., Domingo-Fernandez, R., Johnston, D.G., et al. (2015). Pyruvate kinase M2 regulates Hif-1α activity and IL-1β induction and is a critical determinant of the warburg effect in LPS-activated macrophages. Cell Metab. *21*, 65–80.

Shah, Y.M., and Xie, L. (2014). Hypoxia-inducible factors link iron homeostasis and erythropoiesis. Gastroenterology *146*, 630–642.

Shah, Y.M., Matsubara, T., Ito, S., Yim, S.H., and Gonzalez, F.J. (2009). Intestinal hypoxia-inducible transcription factors are essential for iron absorption following iron deficiency. Cell Metab. *9*, 152–164.

Shinkai, Y., Rathbun, G., Lam, K.P., Oltz, E.M., Stewart, V., Mendelsohn, M., Charron, J., Datta, M., Young, F., Stall, A.M., et al. (1992). RAG-2-deficient mice lack mature lymphocytes owing to inability to initiate V(D)J rearrangement. Cell *68*, 855–867.

Takeda, K., Ho, V.C., Takeda, H., Duan, L.J., Nagy, A., and Fong, G.H. (2006). Placental but not heart defects are associated with elevated hypoxia-inducible factor alpha levels in mice lacking prolyl hydroxylase domain protein 2. Mol. Cell. Biol. *26*, 8336–8346.

Taniguchi, C.M., Finger, E.C., Krieg, A.J., Wu, C., Diep, A.N., LaGory, E.L., Wei, K., McGinnis, L.M., Yuan, J., Kuo, C.J., and Giaccia, A.J. (2013). Cross-talk between hypoxia and insulin signaling through Phd3 regulates hepatic glucose and lipid metabolism and ameliorates diabetes. Nat. Med. *19*, 1325–1330.

Taniguchi, C.M., Miao, Y.R., Diep, A.N., Wu, C., Rankin, E.B., Atwood, T.F., Xing, L., and Giaccia, A.J. (2014). PHD inhibition mitigates and protects against radiation-induced gastrointestinal toxicity via HIF2. Sci. Transl. Med. *6*, 236ra64.

Taylor, M., Qu, A., Anderson, E.R., Matsubara, T., Martin, A., Gonzalez, F.J., and Shah, Y.M. (2011). Hypoxia-inducible factor-2α mediates the adaptive increase of intestinal ferroportin during iron deficiency in mice. Gastroenterology *140*, 2044–2055.

Uehata, T., Iwasaki, H., Vandenbon, A., Matsushita, K., Hernandez-Cuellar, E., Kuniyoshi, K., Satoh, T., Mino, T., Suzuki, Y., Standley, D.M., et al. (2013). Malt1-induced cleavage of regnase-1 in CD4(+) helper T cells regulates immune activation. Cell *153*, 1036–1049.

Vanoaica, L., Darshan, D., Richman, L., Schümann, K., and Kühn, L.C. (2010). Intestinal ferritin H is required for an accurate control of iron absorption. Cell Metab. *12*, 273–282.

Walmsley, S.R., Chilvers, E.R., Thompson, A.A., Vaughan, K., Marriott, H.M., Parker, L.C., Shaw, G., Parmar, S., Schneider, M., Sabroe, I., et al. (2011). Prolyl hydroxylase 3 (PHD3) is essential for hypoxic regulation of neutrophilic inflammation in humans and mice. J. Clin. Invest. *121*, 1053–1063.

Weiss, G., and Goodnough, L.T. (2005). Anemia of chronic disease. N. Engl. J. Med. *352*, 1011–1023.

Wilkinson, N., and Pantopoulos, K. (2014). The IRP/IRE system in vivo: insights from mouse models. Front. Pharmacol. *5*, 176.

Zhou, Z., Miao, R., Huang, S., Elder, B., Quinn, T., Papasian, C.J., Zhang, J., Fan, D., Chen, Y.E., and Fu, M. (2013). MCPIP1 deficiency in mice results in severe anemia related to autoimmune mechanisms. PLoS ONE *8*, e82542.

Zuker, M. (2003). Mfold web server for nucleic acid folding and hybridization prediction. Nucleic Acids Res. *31*, 3406–3415.

**Cell Reports, Volume *19***

## Supplemental Information

# Regnase-1 Maintains Iron Homeostasis via the Degradation of Transferrin Receptor 1 and Prolyl-Hydroxylase-Domain-Containing Protein 3 mRNAs

**Masanori Yoshinaga, Yoshinari Nakatsuka, Alexis Vandenbon, Daisuke Ori, Takuya Uehata, Tohru Tsujimura, Yutaka Suzuki, Takashi Mino, and Osamu Takeuchi**

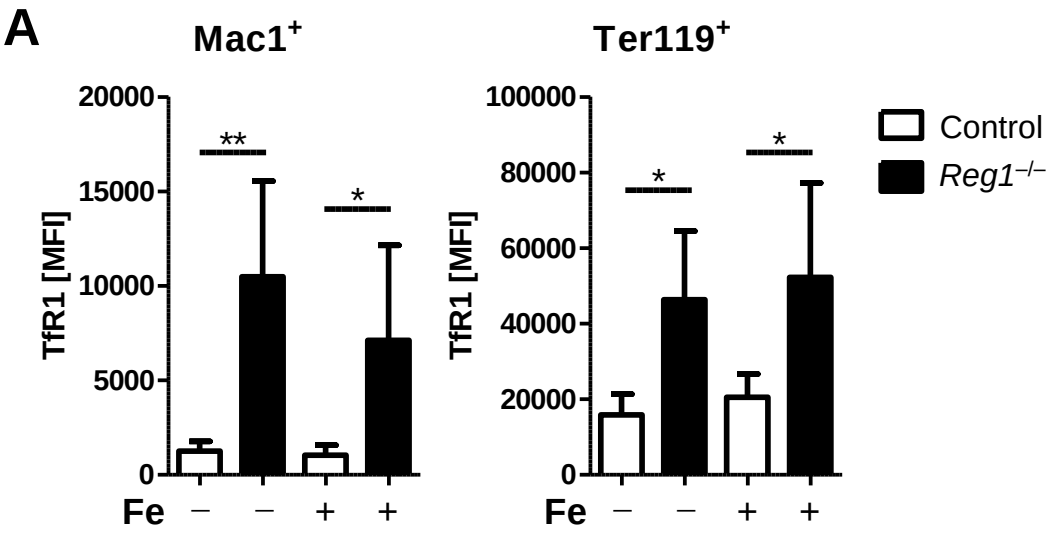


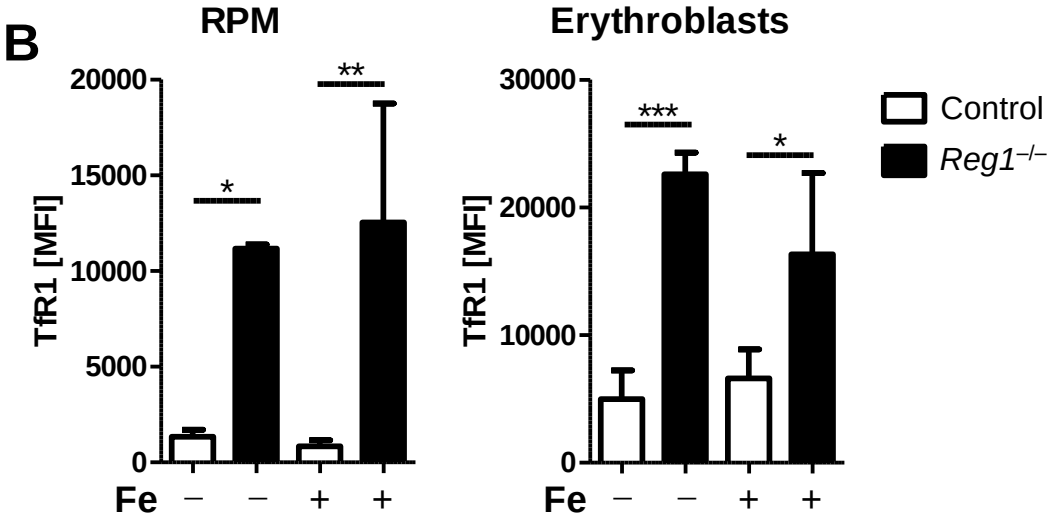


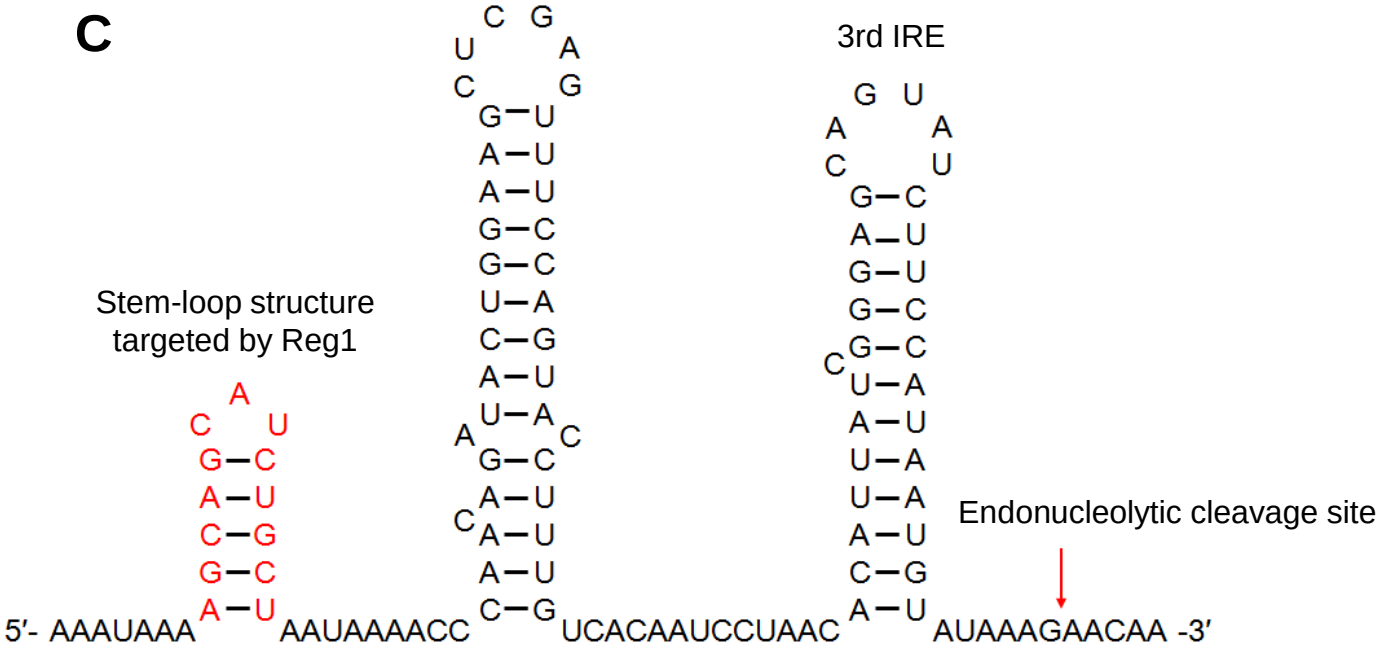


Figure S1. TfR1 expression is elevated in *Reg1*$^{-/-}$ cells even after iron supplementation *in vitro* and *in vivo*

**Figure S1. TfR1 expression is elevated in *Reg1*$^{-/-}$ cells even after iron supplementation, Related to Figure 1.**

(A) Total splenocytes were harvested from control and *Reg1*$^{-/-}$ mice and then cultured in iron-supplemented medium (100μM hemin) for 8 hours. Cells were then harvested, stained and analyzed using flow cytometry. Mac1$^{+}$ or Ter119$^{+}$ populations were gated and the mean fluorescence intensity (MFI) of TfR1 in each gated population was calculated (n=6). Data were pooled from 2 independent experiments.

(B) Control and *Reg1*$^{-/-}$ mice were injected intraperitoneally with saccharated ferric oxide (50mg/kg) 3 times a week for 3 weeks. Then total splenocytes were harvested, stained and analyzed using flow cytometry. CD11b$^{lo}$ F4/80$^{+}$ red pulp macrophages (RPM) and Ter119$^{+}$ erythroblasts were gated and the MFI of TfR1 in each gated population was calculated (n=3-4). Data were pooled from 2 independent experiments.

(C) Secondary structure model of TRS-1 mRNA (partial) (Horowitz and Harford, 1992). TRS-1 is the truncated *TfR1* mRNA used to identify the endonucleolytic cleavage site in the previous study (Binder et al., 1994). The stem-loop structure targeted by Reg1 (Figure 2G) was shown in red. The endonucleolytic cleavage site was derived from Binder *et al.*

Data are expressed as mean ± SD. *p < 0.05, **p < 0.01 in one-way-ANOVA with Bonferroni correction (A and B).

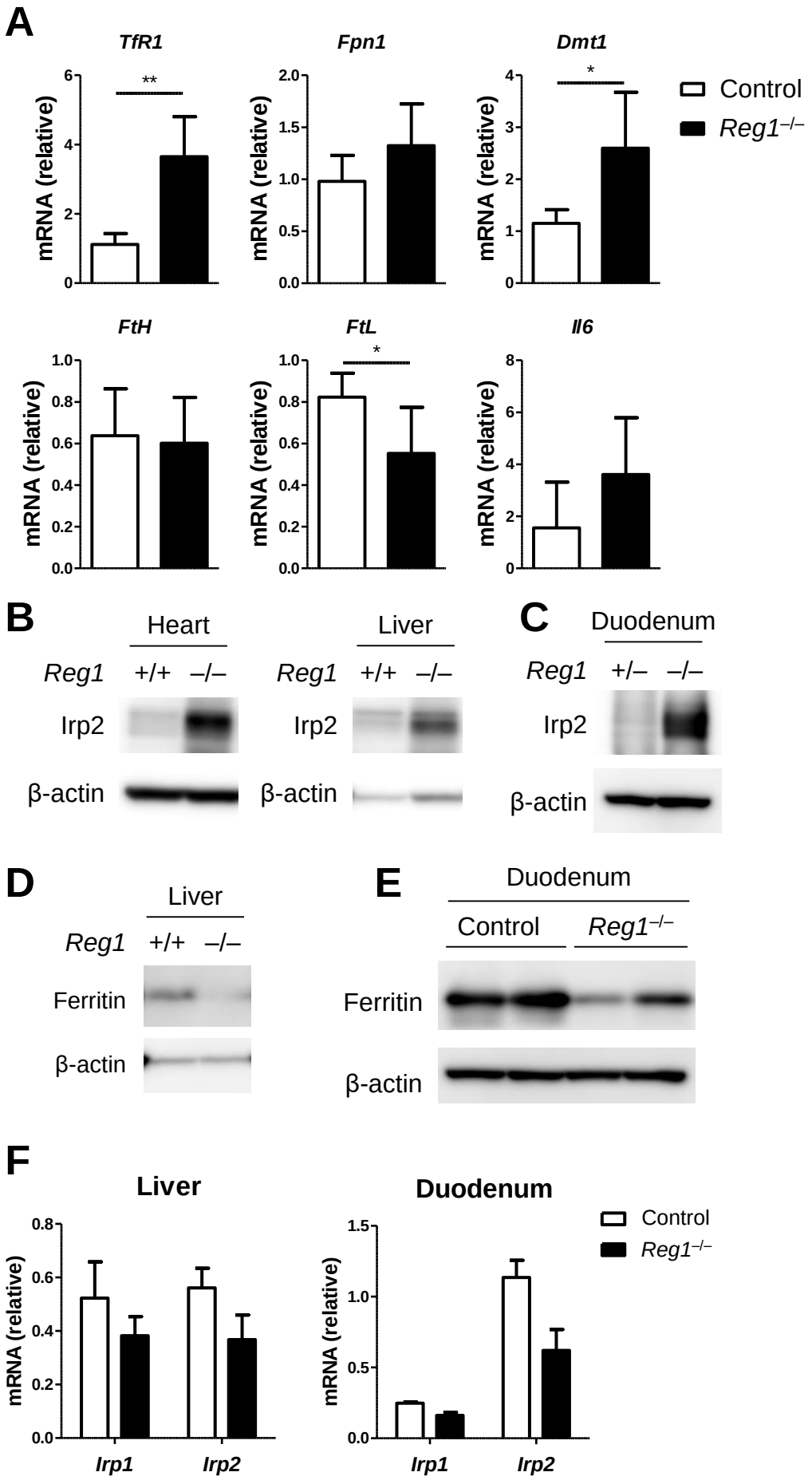


Figure S2. IRP2 is post-translationally upregulated in *Reg1*$^{-/-}$ tissues

**Figure S2. IRP2 is post-translationally upregulated in *Reg1*$^{-/-}$ tissues, Related to Figure 3.**

(A) mRNA expression levels in the liver of control and *Reg1*$^{-/-}$ mice (n=4-5). Data were pooled from two independent experiments.
(B-C) Immunoblot analysis of IRP2 and β-actin in indicated tissues from control and *Reg1*$^{-/-}$ mice. Data are representative of two independent experiments.
(D-E) Immunoblot analysis of ferritin and β-actin in indicated tissues from control and *Reg1*$^{-/-}$ mice. Data are representative of two independent experiments.
(F) mRNA expression levels of *Irp1* and *Irp2* in the liver and duodenum of control and *Reg1*$^{-/-}$ mice (n=3).
Data are expressed as mean ± SD (A and F). *$p < 0.05$ in Student's t test (A).

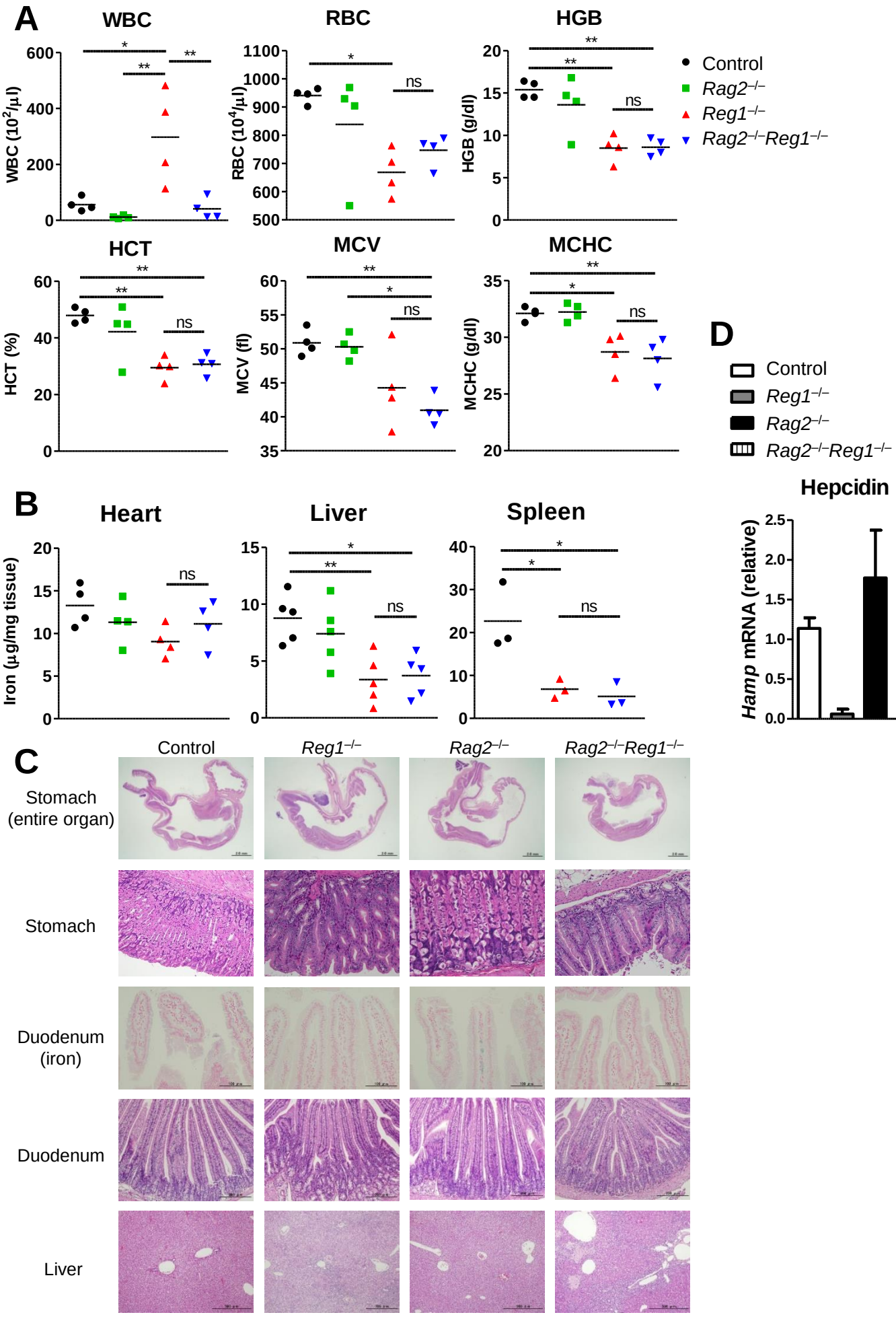


Figure S3. *Reg1*$^{-/-}$ mice develop severe anemia and iron deficiency mainly independent of inflammation

**Figure S3. *Reg1*$^{-/-}$ mice develop severe anemia and iron deficiency mainly independent of inflammation, Related to Figure 3.**

(A) Hematological parameters of control, *Rag2*$^{-/-}$, *Reg1*$^{-/-}$ and *Rag2*$^{-/-}$*Reg1*$^{-/-}$ mice (n=4). WBC, white blood cells; RBC, red blood cells; HGB, hemoglobin; HCT, hematocrit; MCV, mean corpuscular volume; MCHC, mean corpuscular hemoglobin concentration; ns, not significant. Data were pooled from 4 independent experiments.
(B) Iron levels of each organ from control, *Rag2*$^{-/-}$, *Reg1*$^{-/-}$ and *Rag2*$^{-/-}$*Reg1*$^{-/-}$ mice (n=3-5). Data were pooled from 3 independent experiments.
(C) Hematoxylin and eosin stain of the stomach, duodenum and liver and Berlin blue stain of the duodenum from control, *Rag2*$^{-/-}$, *Reg1*$^{-/-}$ and *Rag2*$^{-/-}$*Reg1*$^{-/-}$ mice.
(D) Hepcidin mRNA expression levels in the liver of control, *Rag2*$^{-/-}$, *Reg1*$^{-/-}$ and *Rag2*$^{-/-}$*Reg1*$^{-/-}$ mice (n=3).
Each symbol represents the value from individual mice and Horizontal lines indicate the mean (A and B). Data are expressed as mean ± SD (D). *p < 0.05, **p < 0.01, ***p < 0.001 in one-way-ANOVA with Bonferroni correction (A and B). Representative images of each genotype are shown (C).

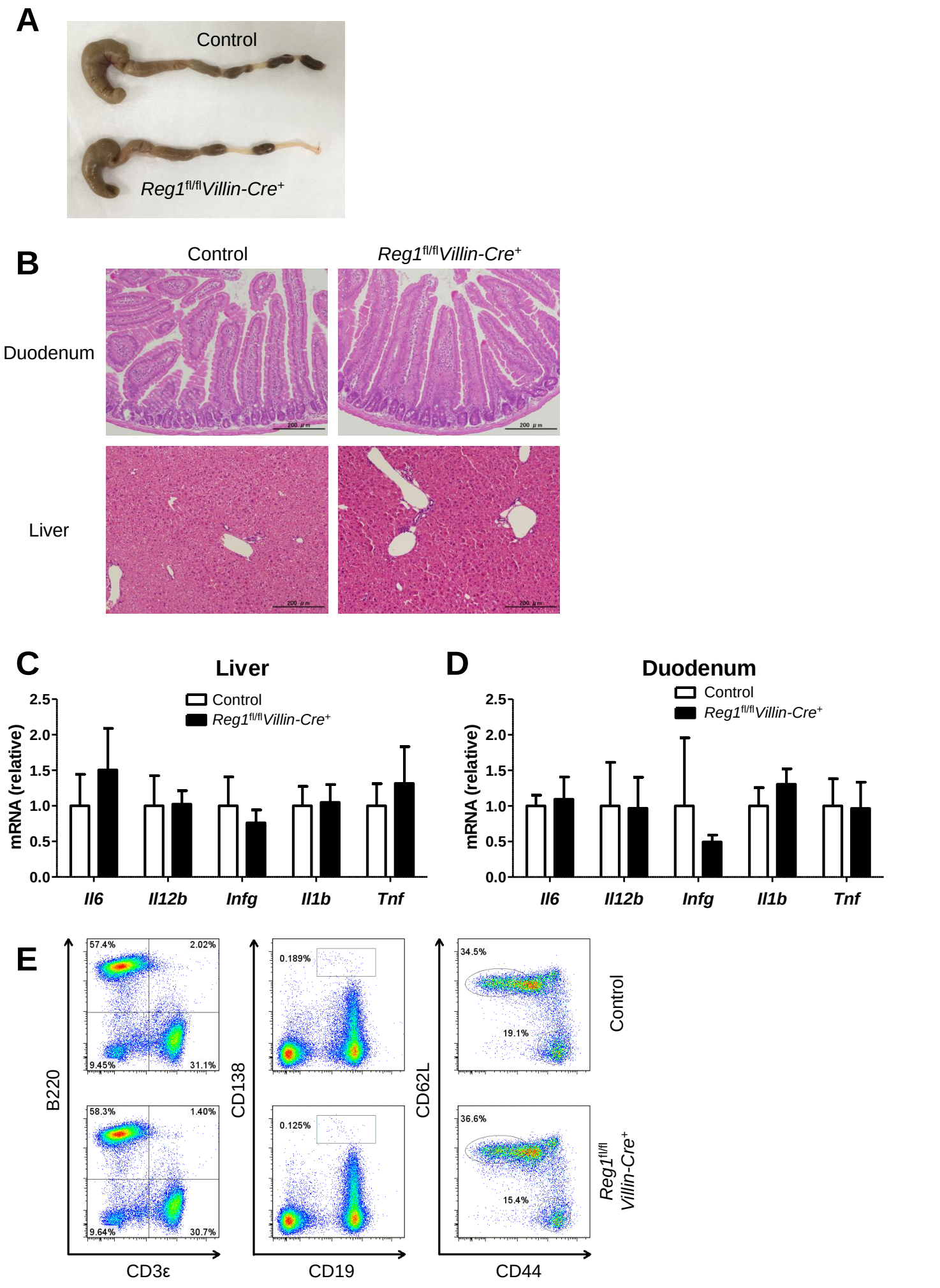


Figure S4. *Reg1*$^{fl/fl}$*Villin-Cre*$^{+}$ mice show no sign of inflammation

**Figure S4. *Reg1*$^{fl/fl}$*Villin-Cre*$^{+}$ mice show no sign of inflammation, Related to Figure 4.**

(A) Macroscopic appearance of the colon from control and *Reg1*$^{fl/fl}$*Villin-Cre*$^{+}$ mice.
(B) Hematoxylin and eosin stain of the duodenum and liver from control and *Reg1*$^{fl/fl}$*Villin-Cre*$^{+}$ mice.
(C-D) mRNA expression levels in the liver (C) and duodenum (D) of control and *Reg1*$^{fl/fl}$*Villin-Cre*$^{+}$ mice (n=5).
(E) Total splenocytes were harvested from control and *Reg1*$^{fl/fl}$*Villin-Cre*$^{+}$ mice, stained and analyzed using flow cytometry as indicated in the figure.
Data are expressed as mean ± SD (C and D). Representative images of each genotype are shown (A, B and E).

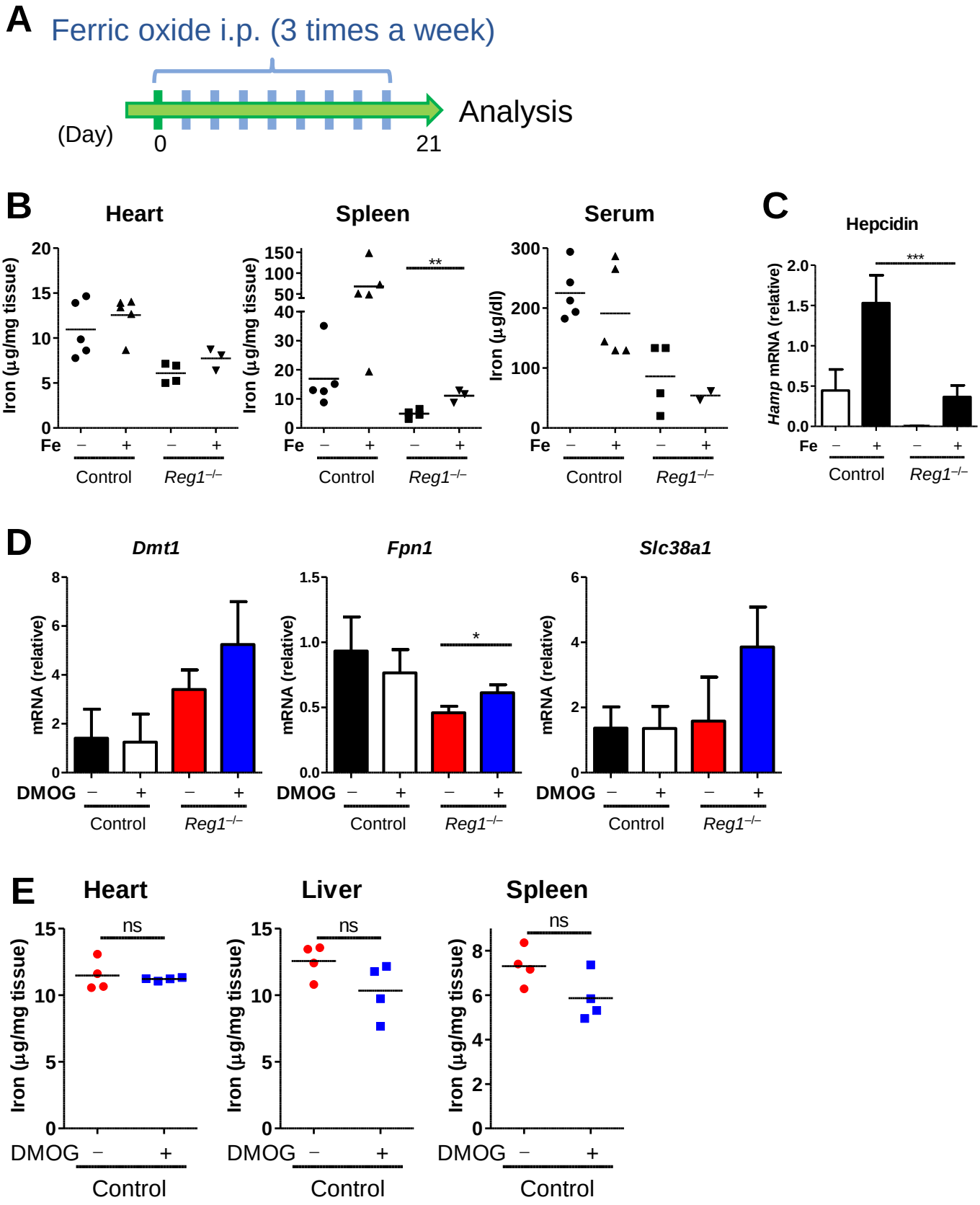


Figure S5. Supplementation of iron or DMOG ameliorates iron deficiency in *Reg1*$^{-/-}$ mice

**Figure S5. Supplementation of iron or DMOG ameliorates iron deficiency in *Reg1*$^{-/-}$ mice, Related to Figure 4.**

(A) The experimental procedure of iron administration into mice. Control and *Reg1*$^{-/-}$ mice were injected intraperitoneally with saccharated ferric oxide (50 mg/kg) 3 times a week for 3 weeks.
(B) Tissue and serum iron levels of control and *Reg1*$^{-/-}$ mice treated with saline or iron (n=2-5).
(C) Hepatic hepcidin mRNA expression levels in control and *Reg1*$^{-/-}$ mice after the iron treatment (n=3-5). Data were pooled from two independent experiments.
(D) mRNA levels of HIF2α target genes in the duodenum of control and *Reg1*$^{-/-}$ mice treated with DMOG or saline for 6 h (n=3-4). Data were pooled from two independent experiments.
(E) Tissue iron levels of age-matched wild-type mice treated with DMOG or saline for 2 weeks (n=4).
Each symbol represents the value from individual mice. Horizontal lines indicate the mean (B and E). Data are expressed as mean ± SD (C and D). *p < 0.05, **p < 0.01, ***p < 0.001 in Student's t test (D and E) or in one-way-ANOVA with Bonferroni correction (B and C). ns, not significant.

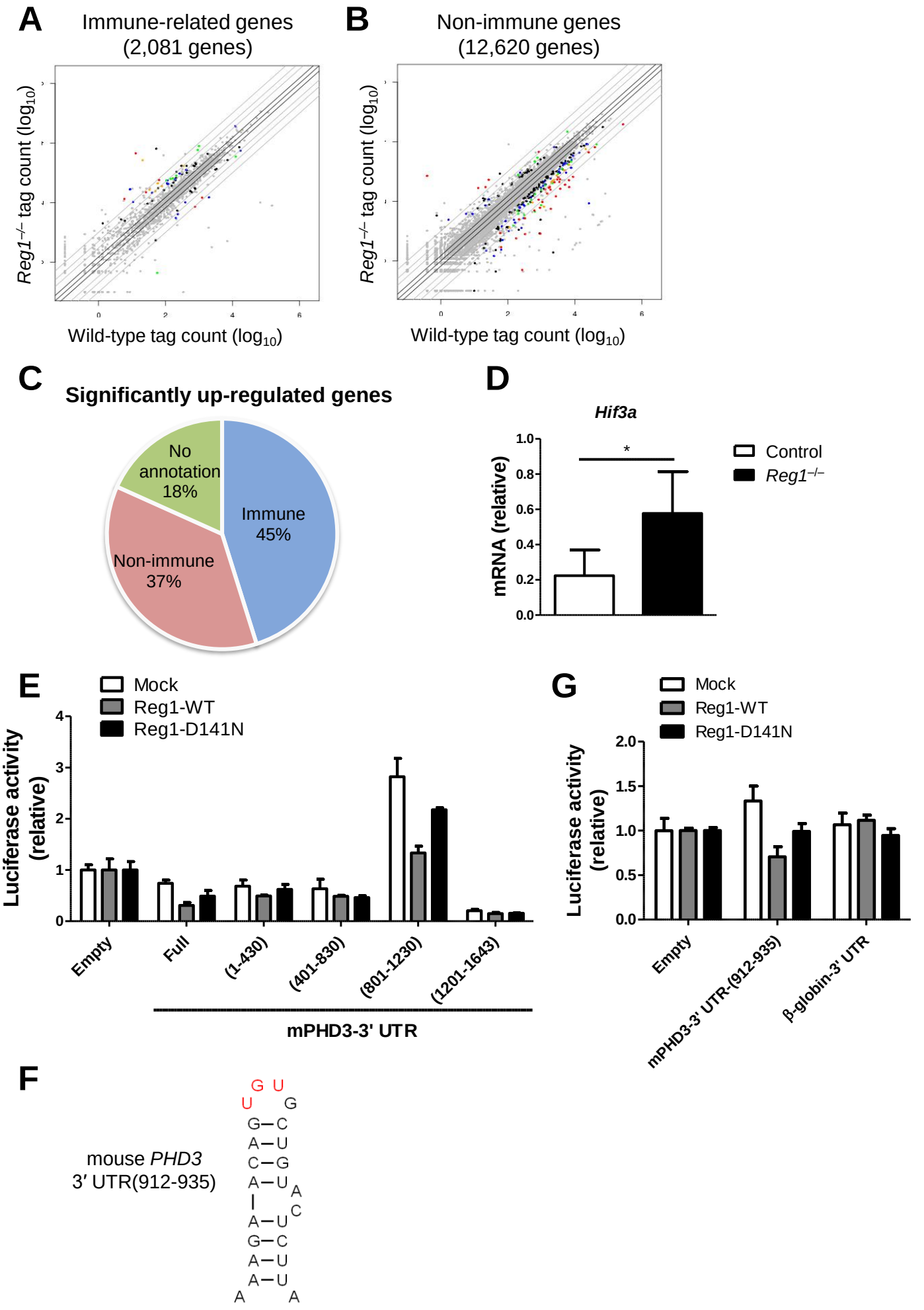


Figure S6. Identification and validation of Reg1 target genes in the duodenum

**Figure S6. Identification and validation of Reg1 target genes in the duodenum, Related to Figure 5.**

(A-C) Total RNA was harvested from *Reg1*$^{-/-}$ and control duodenums (n=2), and subjected to transcriptome analysis. Immune-related genes and non-immune genes were selected based on the GO analysis (see Extended Experimental Procedures). Scatter plot comparing the expression of immune-related genes (2,081 genes, A) and non-immune genes (12,620 genes, B) in the duodenum from wild-type and *Reg1*$^{-/-}$ mice, and classification of significantly up-regulated genes in *Reg1*$^{-/-}$ duodenum based on the GO analysis (C) were shown.
(D) *Hif3a* mRNA levels in the duodenum of control and *Reg1*$^{-/-}$ mice (n=4).
(E-G) HEK293T cells were co-transfected with a series of luciferase reporter plasmids and the expression plasmids for wild-type Reg1 (Reg1-WT), mutant Reg1 (Reg1-D141N), or empty plasmid as a control (Mock). After 48 h of incubation, the luciferase activity of cell lysates was determined (E and G). The predicted stem-loop structure of mouse *PHD3* 3′ UTR (912-935). The canonical pyrimidine-purine-pyrimidine loop is indicated as red (F).
Data are expressed as mean ± SD of biological replicates (D) or triplicates (E and G). *$p < 0.05$ in Student's t test (D).

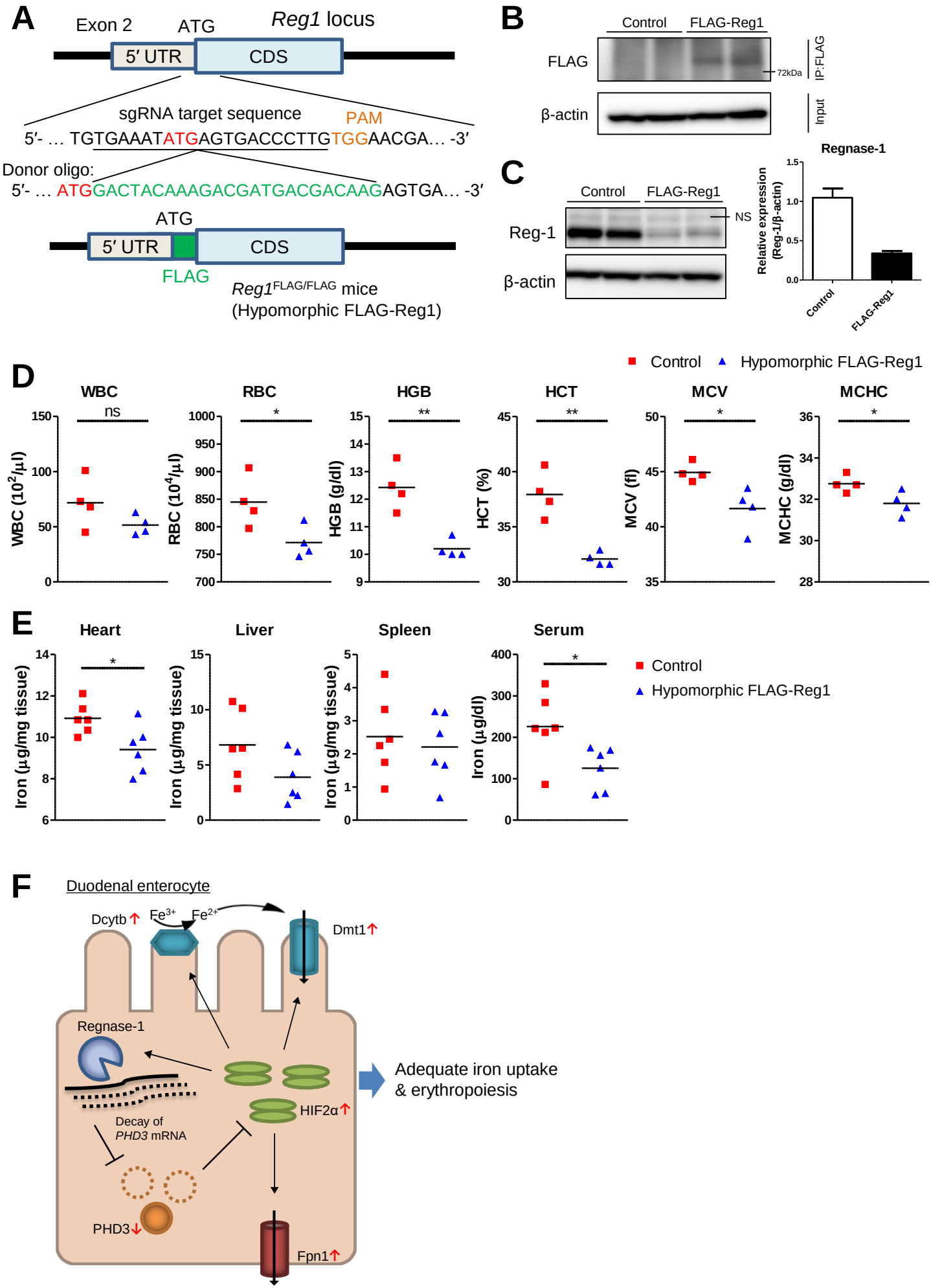


Figure S7. The role of the regulation of Reg1 expression in iron homeostasis

**Figure S7. The role of the regulation of Reg1 expression in iron homeostasis, Related to Figure 7.**

(A) Scheme of the generation of FLAG-Reg1 knock-in mice. Gene-editing strategy mediated by CRISPR/Cas9 system was used to insert the FLAG sequence into 5′ end of Reg1 coding sequence. The resulting mice were used as a Reg1 hypomorphic strain.
(B) Immunoblot analysis of FLAG-Reg1 and β-actin in the duodenal epithelial cells from control and FLAG-Reg1 mice (n=2). Duodenal epithelial cells were subjected to immunoprecipitation with anti-FLAG antibody, followed by immunoblotting.
(C) Immunoblot analysis of Reg1 and β-actin in the duodenal epithelial cells from control and FLAG-Reg1 mice (n=2). NS, non-specific band.
(D) Hematological parameters of control and hypomorphic FLAG-Reg1 mice at the age of 3-4 weeks (n=4). WBC, white blood cells; RBC, red blood cells; HGB, hemoglobin; HCT, hematocrit; MCV, mean corpuscular volume; MCHC, mean corpuscular hemoglobin concentration; ns, not significant.
(E) Tissue and serum iron levels of control and hypomorphic FLAG-Reg1 mice at the age of 3-4 weeks (n=6). Data were pooled from 3 independent experiments.
(F) Model of Reg1-mediated regulation of iron uptake in the duodenum.
Each symbol represents the value from individual mice. Horizontal lines indicate the mean (D and E). *$p < 0.05$, **$p < 0.01$, ***$p < 0.001$ in Student's t test (D and E). ns, not significant.

## Supplemental Experimental Procedures

### Mice and Treatment

*Regnase-1*$^{-/-}$ (*Reg1*$^{-/-}$), *Reg1*$^{fl/fl}$, *Rag2*$^{-/-}$, *PHD3*$^{-/-}$ and *Villin-Cre* transgenic mice have been described previously (el Marjou et al., 2004; Matsushita et al., 2009; Shinkai et al., 1992; Takeda et al., 2006; Uehata et al., 2013). *Rag2*$^{-/-}$ or *PHD3*$^{+/-}$ mice were crossed with *Reg1*$^{+/-}$ mice to obtain *Rag2*$^{+/-}$*Reg1*$^{+/-}$ or *PHD3*$^{+/-}$ *Reg1*$^{+/-}$ mice, respectively. The resulting mice were intercrossed to generate the double knockout mice. *Reg1*$^{fl/fl}$ mice were crossed with *Villin-Cre* transgenic mice. Unless otherwise specified, wild-type, heterozygous or Cre-negative mice were used as controls. All animal experiments were conducted in compliance with the regulations approved by the Committee for Animal Experiments of the Institute for Virus Research or the Institute for Frontier Life and Medical Sciences, Kyoto University.

To directly administer iron *in vivo*, mice were injected intraperitoneally with saccharated ferric oxide (50 mg/kg, Nichi-Iko) 3 times a week for 3 weeks. The non-toxic dose was estimated according to Mencacci *et al.* (Mencacci et al., 1997).

To rescue the HIF activity *in vivo*, we followed the method administering HIF hydroxylase inhibitor, dimethyloxaloylglycine (DMOG), with a slight modification from that of Forristal *et al.* (Forristal et al., 2013). *Reg1*$^{-/-}$ and age-matched wild-type mice were intraperitoneally administered DMOG diluted in PBS (400mg/kg) 3 times a week for 2 weeks.

To induce iron deficiency in mice, mice were fed with low-iron diet (3.4 ppm, Clea) for 4 weeks. This treatment was sufficient to induce iron-deficiency anemia as shown in Figure 6A.

### Generation of Hypomorphic FLAG-Reg1 Mice

The FLAG-Reg1 knock-in mice were generated by using clustered regularly interspaced short palindromic repeats/CRISPR-associated proteins 9 (CRISPR/Cas9)-mediated genome-editing technology as previously described (Fujihara and Ikawa, 2014). Briefly, pX330 humanized Cas9/synthetic guide RNA (sgRNA) expressing plasmid (Addgene) was digested with *Bbs*I, and ligated with annealed sgRNA oligos targeting the 5′ end of Reg1 coding sequence. The constructed pX330 plasmid was suspended in PBS together with the donor single strand oligo which contains FLAG coding sequence, and injected into fertilized eggs of C57BL/6J mice. Successful insertion was confirmed by direct sequencing.

### Reagents and Cells

Antibodies for immunoblot analysis were as follows: HRP anti-β-actin (C-11; Santa Cruz Biotechnology), anti-PHD3 (NB100-303; Novus Biologicals), anti-ferroportin (MTP11-A; Alpha Diagnostic International) anti-ferritin (ab75973; Abcam), and anti-FLAG (F3165 and F7425; Sigma). The monoclonal anti-IRP2 antibody was kindly provided by K. Iwai (Kyoto University). The polyclonal rabbit antibody for Reg1 has been described (Iwasaki et al., 2011). Secondary HRP-conjugated antibodies were from GE Healthcare.

Antibodies for FACS analysis were from BD Biosciences, BD Pharmingen or BioLegend. Actinomycin D (ActD), doxycycline hyclate (Dox), hemin, deferoxamine mesylate (DFO) and Nitrotetrazolium Blue chloride were purchased from Sigma. DMOG was purchased from Calbiochem. G418 disulfate and 2-mercaptoethanol were from Nacalai Tesque. RNasin was from Promega. Complete Mini Protease Inhibitor Cocktail was from Roche. Media for cell culture were from Nacalai Tesque unless otherwise specified.

Isolation of peritoneal exudate cells (PECs) was described previously (Matsushita et al., 2009). PECs were cultured in RPMI-1640 medium supplemented with 10% FBS, 100 U/ml of penicillin, 100 μg/ml of streptomycin and 50 μM 2-mercaptoethanol. Bone marrow cells were isolated from tibia and femur. HEK293T cells were cultured in Dulbecco's modified eagle medium (DMEM) supplemented with 10% FBS, 100 U/ml of penicillin, 100 μg/ml of streptomycin and 50 μM 2-mercaptoethanol. Tet-off HEK293 cells were purchased from Clontech and cultured in α-MEM supplemented with 10% Tet-approved FBS (Clontech), 100 U/ml of penicillin, 100 μg/ml of streptomycin and 100 μg/mL of G418. HCT116 cells were cultured in McCoy's 5A medium (Invitrogen) supplemented with 10% FBS, 100 U/ml of penicillin and 100 μg/ml of streptomycin.

To perform the experiment of *ex vivo* splenocyte treatment, harvested splenocytes were incubated overnight in the medium supplemented with 100 μM hemin.

Cells were transfected through the use of Lipofectamine 2000, 3000 or LTX (Invitrogen) or PEI Max (Polysciences) according to the manufacturer's instructions.

**Plasmids**

The plasmids expressing wild-type and mutant Reg1 have been described (Matsushita et al., 2009). pXSSRα-IRP1 and pXSSRα-IRP2 were kindly provided by K. Iwai (Kyoto University). pcDNA3-HIF1α-P402A/P564A and pcDNA3.1-HIF2α-P531A expressing constitutively active HIF1α and HIF2α were provided by E. Nakamura (Kyoto University). p5HRE-Luc was a gift from H. Harada (Kyoto University) (Harada et al., 2005). Full-length 3′ UTR of mouse and human *TfR1*, and mouse *PHD3*, parts (768-1525, 768-940, 768-960) of mouse *TfR1* 3′ UTR, and parts (1-430, 401-830, 801-1230, 1201-1643) of mouse *PHD3* 3′ UTR were inserted into pGL3-promoter vector. A part (944-958) of mouse *TfR1* 3′ UTR and a part (912-935) of mouse *PHD3* 3′ UTR were added to the end of β-globin 3′ UTR and inserted into pGL3-promoter vector through the use of DNA Ligation Kit Ver. 2.1 (Takara). Mouse *TfR1* and *PHD3* CDS+3′ UTR were inserted into pTREtight vector (Clontech). Mouse Reg1 promoter regions (-500-TSS, -200-TSS) were inserted into pGL4.10 vector. The deletion of the putative hypoxia-response element (HRE2) was conducted through the use of QuikChange Site-Directed Mutagenesis Kit (Agilent). Cloning was performed using In-Fusion HD Cloning Kit (Clontech) unless otherwise specified.

**Flow Cytometric Analysis**

To obtain single-cell suspension of splenocytes, spleens from mice were homogenized, treated with Red

Blood Cell Lysing Buffer (Sigma), and resuspended in MACS buffer (0.5% BSA (Sigma), 2 mM EDTA and 1× DPBS). Then cells were stained with fluorescent-labeled antibodies for 15 min, washed and resuspended in MACS buffer. Flow cytometric data were collected using FACSVerse (BD Biosciences). Collected data were analyzed with FlowJo (TreeStar).

**Tissue Harvest**

Liver, heart, spleen, stomach, kidney and colon were resected *en bloc* at necropsy. As for the duodenum, the gastrointestinal tract between pyloric sphincter and 1 cm distal part from the sphincter was collected. Organs were processed immediately for western blot analysis and tissue iron measurement, or stored at -80 °C in RNAlater (Qiagen) for RNA isolation according to the manufacturer's instructions.

**Isolation of Duodenal Epithelial Cells**

To isolate duodenal epithelial cells, we followed the method of Nowarski *et al.* (Nowarski et al., 2015). Proximal duodenums were harvested, cut longitudinally, and washed in DPBS. Duodenums were placed in Dissociation Buffer 1 (30mM EDTA, 1.5mM DTT in 1× DPBS) on ice for 20 min. Then duodenums were placed in Dissociation Buffer 2 (30mM EDTA in 1× DPBS) 37 °C for 10 min. To release epithelium, duodenums were vigorously shaked (2.5-3.5 g, 90 cycles for 30 sec). Then remnant intestinal tissues were removed. The detached epithelium was collected by centrifugation and homogenized in TRIzol (Invitrogen) or RIPA buffer (1% Nonidet P-40, 1% SDS, 1% sodium deoxycholate, 150 mM NaCl, 20 mM Tris-HCl (pH 8.0), 10 mM EDTA and Complete Mini Protease Inhibitor Cocktail).

**Immunoblot Analysis**

Whole-cell extracts of tissue samples were prepared in RIPA buffer. Samples were mixed with sample buffer, boiled at 95 °C for 5 min and cooled on ice. For the detection of ferroportin, samples were not boiled. Samples were loaded on either 5-20%, 7.5% or 15% polyacrylamide gel (ATTO), electrophoresed, and transferred to PVDF membranes (Bio-Rad). The membranes were immersed in 5% skim milk (BD Difco) in TBS-T. Signal Enhancer HIKARI for Western Blotting and ELISA (Nacalai Tesque), Can Get Signal Immunoreaction Enhancer Solution (Toyobo) or 5% skim milk in TBS-T was used to dilute primary and secondary antibodies. Blots were developed using Luminata Forte Western HRP Substrate (Millipore) according to the manufacturer's instructions. Chemiluminescent detection was performed using ImageQuant LAS 4000 or Amersham Imager 600 (GE Healthcare). Densitometric analysis was performed through the use of NIH ImageJ software.

**Quantitative PCR Analysis**

TRIzol (Invitrogen) or ISOGEN (Nippongene) was used for the isolation of total RNA, and ReverTra Ace with gDNA Remover (Toyobo) was used for cDNA synthesis according to the manufacturer's instructions.

For quantitative PCR, the synthesized cDNAs were amplified using Thunderbird SYBR qPCR Mix (Toyobo), or Universal SYBR Select Master Mix or PowerUp SYBR Green Master Mix (Applied Biosystems) according to the manufacturer's instructions. Fluorescence was detected using 7500 real-time PCR system (Applied Biosystems). To determine the relative expression, mRNA expression levels of genes were normalized to the expression level of glyceraldehyde 3-phosphate dehydrogenase (*Gapdh*) or β-actin (*Actb*).

**RNA Sequencing and Bioinformatics Analysis**

Proximal duodenums were immersed in TRIzol (Invitrogen) and immediately homogenized using VH-10 (AS ONE). Then total RNA was extracted according to the manufacturer's instructions. Transcriptome data were collected as described previously (Uehata et al., 2013). The method DESeq was utilized to estimate significant differentially expressed genes between wild-type and *Reg1*$^{-/-}$ duodenums (duplicate samples) (Anders and Huber, 2010). Immune-related genes were defined based on Gene Ontology (GO) annotation terms. Gene ontologies (basic and GOslim; date 11/01/2015) and mouse annotations (GOC validation date 09/01/2015) were downloaded from the Gene Ontology Consortium website (Ashburner et al., 2000). Immune-related genes were defined as genes associated with one or more of the following GO terms: GO:0002376 ("immune system process"), GO:0002682 ("regulation of immune system process"), GO:0006954 ("inflammatory response"), GO:0050727 ("regulation of inflammatory response"), GO:0042742 ("defense response to bacterium") and GO:0034097 ("response to cytokine"), or any of their respective child annotations. Top-ranked up-regulated genes with non-immune-related annotations were sorted by adjusted p value after excluding the immune-related genes and genes without definitions.

HREs were predicted in the Reg1 promoter by scanning them with the corresponding position weight matrix (PWM) from the Jaspar database (matrix ID: MA0259.1) (Mathelier et al., 2014). A PWM threshold score was set in a way that results in about one predicted binding site per 5kb of the mouse genome (mm10). Scanning of the region -500 to -1 relative to the Reg1 TSS resulted in two significant hits for the HRE.

**Analysis of Microarray Datasets**

Microarray datasets (GSE14891) have been described (Matsushita et al., 2009). These datasets were used to calculate robust multichip average (RMA) expression values as previously described (Matsushita et al., 2009). The reprocessed data shown in Table S1 were utilized to compare the difference in mRNA expression at 0 h (without any stimulation) between wild-type and *Reg1*$^{-/-}$ PECs.

**Hematological Analysis**

Blood was collected from retro-orbital plexus of anesthetized mice. Blood for hematological analysis was collected into EDTA-2Na-containing tube (Capiject, Terumo Medical). Hematological analyses were

performed using Celltac α hematology analyzers (MEK 6450, Nihon Kohden).

**Tissue and Serum Iron Quantification**

Tissue and serum iron quantification was conducted using Metalloassay Kit (Ferrozine method) according to the manufacturer's instructions (MG Metallogenics). Tissue homogenates were mixed with 1M $HNO_3$ until the pH reached 2, and spun down to obtain the supernatant. Samples were mixed with R-A Buffer and the baseline absorbance of 570 nm of samples was determined ($OD_A$) using iMark Microplate Absorbance Reader (BioRad). Then R-R Chelate Color was added to the samples, and after 5 min of reaction, the absorbance of 570 nm was again determined ($OD_B$). To measure iron concentration in samples, the increase in absorbance, $OD_B$-$OD_A$, was calculated and compared with the standard curve.

**Determination of Unbound Iron Binding Capacity and Total Iron Binding Capacity**

Unbound iron binding capacity (UIBC) was determined using Microassay UIBC Kit (MG Metallogenics) according to the manufacturer's instructions. Absorbance of 546 nm and 600 nm of samples was determined using Nanodrop 2000c Spectrophotometers (Thermo Fisher Scientific). Total iron binding capacity (TIBC) was determined by adding UIBC to serum iron values.

**Ferric Reductase Assay**

Ferric reductase assay was performed as previously described (Shah et al., 2009). In brief, proximal duodenums were washed in ice-cold 150mM NaCl, and incubated in Incubation Buffer (125mM NaCl, 3.5mM KCl, 16mM HEPES/NaOH, and 1mM Nitrotetrazolium blue chloride) at 37 °C. Then the reaction was halted by washing the duodenum in ice-cold 150mM NaCl twice.

**Histological Analysis**

Tissue samples were fixed with 10% formalin solution or 4% paraformaldehyde/PBS. Tissue-iron detection was performed in formalin fixed paraffin-embedded sections stained with Berlin blue.

**RNA Secondary Structure Prediction**

The mfold program was used for RNA secondary structure predictions (Zuker, 2003).

**Luciferase Assay**

To identify Reg1 targets in 3′ UTR, HEK293T cells were co-transfected with luciferase reporter plasmid (pGL3 vector) and the expression plasmids for wild-type or mutant Reg1, or empty plasmid as a control. After 48 h of incubation, cells were lysed.

For promoter assay, HCT116 cells were co-transfected with luciferase reporter plasmids harboring mouse Reg1 promoter regions (pGL4.10 vector) and the expression plasmids for constitutively

active HIF1α (P402A/P564A) or HIF2α (P531A), or empty plasmid as a control. After 24 h of incubation, cells were lysed.

Luciferase activity was determined with the Dual-Luciferase Reporter Assay system (Promega) and GloMax-Multi Detection System (Promega). The gene encoding *renilla* luciferase was transfected simultaneously as an internal control.

**mRNA Decay Assay**

To analyze mRNA decay using the Tet-Off system (Clontech), Tet-Off HEK293 cells were transfected with the pTREtight vector harboring full-length of mouse *TfR1* or *PHD3* CDS+3′ UTR, together with the expression vectors of wild-type Reg1 or control (Mock). After overnight incubation, cells were treated with Dox (1 μg/ml) and total RNA was harvested at the indicated time points.

To analyze mRNA decay using primary cells, PECs from control and *Reg1*$^{-/-}$ mice were treated overnight with DFO (100 μM). The cells were then treated with ActD (1 μg/ml) and hemin (100 μM). Total RNA was harvested at the indicated time points following the treatment.

**RNA Immunoprecipitation**

HEK293T cells were transfected with the expression vector for mutant Reg1 (D141N), or empty plasmid as a control. After 48h of incubation, medium was removed, followed by UV cross-linking using CL-1000 (UVP). Cells were lysed in RIP Lysis buffer (20 mM Tris-HCl (pH 7.4), 100mM KCl, 1.5 mM $MgCl_2$, 0.5% NP-40, 0.2 U/mL RNasin and Complete Mini Protease Inhibitor Cocktail). Lysates were aliquoted to obtain input samples. Then cell lysates were mixed with Dynabeads Protein G (Novex) preincubated with anti-FLAG antibody and incubated at 4 °C for 2 h with gentle rotation. Then beads were immobilized, washed 5 times in RIP Wash buffer (20 mM Tris-HCl (pH 7.4), 150 mM KCl, 2.5 mM $MgCl_2$, 0.2 U/mL RNasin and Complete Mini Protease Inhibitor Cocktail), and mixed with TRIzol (Invitrogen).

**Immunoprecipitation of FLAG-Reg1**

Duodenal epithelial cells were lysed in RIP Lysis buffer (20 mM Tris-HCl (pH 7.4), 100mM KCl, 1.5 mM $MgCl_2$, 0.5% NP-40 and Complete Mini Protease Inhibitor Cocktail). Lysates were aliquoted to obtain input samples. Then cell lysates were mixed with Dynabeads Protein G (Thermo Fisher Scientific) preincubated with anti-FLAG antibody and incubated at 4 °C for 8 h with gentle rotation. Then beads were immobilized, washed 5 times in RIP Lysis buffer, and mixed with sample buffer.

**Statistical Analysis**

Results were expressed as mean ± SD. Statistical analyses were performed using Prism v.5 (GraphPad). Statistical significance was calculated with either two-tailed Student's t-test or one-way ANOVA with Bonferroni correction. P values of less than 0.05 were considered significant. *$p < 0.05$, **$p < 0.01$, ***p

< 0.001, #p < 0.05, ##p < 0.01, ###p < 0.001 were indicated.

**RT-qPCR primers used in this study**

| **Species** | **Gene symbol** | **Forward primer** | **Reverse primer** |
|---|---|---|---|
| *Mus musculus* | *Gapdh* | AGGTCGGTGTGAACGGATTTG | TGTAGACCATGTAGTTGAGGTCA |
| *Mus musculus* | *Actb* | GGCTGTATTCCCCTCCATCG | CCAGTTGGTAACAATGCCATGT |
| *Mus musculus* | *Reg1* | CGAGAGGCAGGAGTGGAAAC | CTTACGAAGGAAGTTGTCCAGGCTAG |
| *Mus musculus* | *Il-6* | GTAGCTATGGTACTCCAGAAGAC | ACGATGATGCACTTGCAGAA |
| *Mus musculus* | *Hamp* | CTACAGAGCTGCAGCCTTTG | GCAACAGATACCACACTGGGAATTG |
| *Mus musculus* | *Epo* | CTCACTTCACTGCTTCGGGT | GGAGGAAGTTGGCGTAGACC |
| *Mus musculus* | *Erfe* | TCTACAGGCAGGACACTACACT | TCACAGGCCCAGGAGGATAG |
| *Mus musculus* | *TfR1* | GCTAGTGTCAGAAAACCCAAGAGG | GTTTCAGCCAGTTTCACACACTCC |
| *Mus musculus* | *Fpn1* | GACAGCTGTCTATGGACTGGTGG | GCAGAGGATGACGGACACATTC |
| *Mus musculus* | *Dmt1* | CCACTGGAGACTCTGAGGAG | CTGGGTCTAGGTAGGCAATGCTC |
| *Mus musculus* | *Dcytb* | GCAGCGGGCTCGAGTTTAACTG | CAGCGTTTAACCCGGCATGG |
| *Mus musculus* | *FtL* | GTGAACCGCCTGGTCAACTTG | CTCGGCCAATTCGCGGAAGAAG |
| *Mus musculus* | *FtH* | CCATCAACCGCCAGATCAACC | CTCCTCATGAGATTGGTGGAGAAAG |
| *Mus musculus* | *PHD1* | AGGCTATGTCCGTCACGTTG | TGGGCTTTGCCTTCTGGAAA |
| *Mus musculus* | *PHD2* | GTAGAAGGTCACGAGCCAGG | ATTGCCTGGATAACACGCCA |
| *Mus musculus* | *PHD3* | ATGGTGATGGCCGCTGTATC | CTGCGGTCTGACCAGAAGAA |
| *Mus musculus* | *Hif3a* | CACTGCTCAGGACATATGAG | TCCAAAGCGTGGATGTATTC |
| *Mus musculus* | *Slc38a1* | GAGCTAACGGAGCTGCAGAAC | CTGTTTGTGAGACTCCTCCTACTCTC |
| *Mus musculus* | *Irp1* | AACACCAGCAATCCATCCGT | GGTGACCACTCCACTTCCAG |
| *Mus musculus* | *Irp2* | TTTGCTGCTATGAGGGAGGC | ACCTCCAGGATTTGGTGCAT |
| *Mus musculus* | *Il12b* | TGGTTTGCCATCGTTTTGCTG | ACAGGTGAGGTTCACTGTTTCT |
| *Mus musculus* | *Ifng* | TGAGTATTGCCAAGTTTGAGGTCA | CGGCAACAGCTGGTGGAC |
| *Mus musculus* | *Il1b* | GCAACTGTTCCTGAACTCAACT | ATCTTTTGGGGTCCGTCAACT |
| *Mus musculus* | *Tnf* | CCCTCACACTCAGATCATCTTCT | GCTACGACGTGGGCTACAG |
| *Homo sapiens* | *GAPDH* | GTTGCCATCAATGACCCCTTCATTG ACC | CAGCATCGCCCCACTTGATTTTGG |
| *Homo sapiens* | *ACTB* | CACCATTGGCAATGAGCGGTTCC | CTTCTGCATCCTGTCGGCAATGC |
| *Homo sapiens* | *18S* | CGGACAGGATTGACAGATTG | CAAATCGCTCCACCAACTAA |
| *Homo sapiens* | *TfR1* | CTGCCAGCCCACTGTTGTAT | GCCCAGTTGCTGTCCTGATA |
| *Homo sapiens* | *PHD3* | CATCGACAGGCTGGTCCTCTA | CCACGTGGCGAACATAACC |

**Supplemental References**

Anders, S., and Huber, W. (2010). Differential expression analysis for sequence count data. Genome Biol 11, R106.

Ashburner, M., Ball, C.A., Blake, J.A., Botstein, D., Butler, H., Cherry, J.M., Davis, A.P., Dolinski, K., Dwight, S.S., Eppig, J.T., et al. (2000). Gene ontology: tool for the unification of biology. The Gene Ontology Consortium. Nat Genet 25, 25-29.

Binder, R., Horowitz, J.A., Basilion, J.P., Koeller, D.M., Klausner, R.D., and Harford, J.B. (1994). Evidence that the pathway of transferrin receptor mRNA degradation involves an endonucleolytic cleavage within the 3' UTR and does not involve poly(A) tail shortening. EMBO J 13, 1969-1980.

el Marjou, F., Janssen, K.P., Chang, B.H., Li, M., Hindie, V., Chan, L., Louvard, D., Chambon, P., Metzger, D., and Robine, S. (2004). Tissue-specific and inducible Cre-mediated recombination in the gut epithelium. Genesis 39, 186-193.

Forristal, C.E., Winkler, I.G., Nowlan, B., Barbier, V., Walkinshaw, G., and Levesque, J.P. (2013). Pharmacologic stabilization of HIF-1alpha increases hematopoietic stem cell quiescence in vivo and accelerates blood recovery after severe irradiation. Blood 121, 759-769.

Fujihara, Y., and Ikawa, M. (2014). CRISPR/Cas9-based genome editing in mice by single plasmid injection. Methods Enzymol 546, 319-336.

Harada, H., Kizaka-Kondoh, S., and Hiraoka, M. (2005). Optical imaging of tumor hypoxia and evaluation of efficacy of a hypoxia-targeting drug in living animals. Mol Imaging 4, 182-193.

Horowitz, J.A., and Harford, J.B. (1992). The secondary structure of the regulatory region of the transferrin receptor mRNA deduced by enzymatic cleavage. New Biol 4, 330-338.

Iwasaki, H., Takeuchi, O., Teraguchi, S., Matsushita, K., Uehata, T., Kuniyoshi, K., Satoh, T., Saitoh, T., Matsushita, M., Standley, D.M., et al. (2011). The IkappaB kinase complex regulates the stability of cytokine-encoding mRNA induced by TLR-IL-1R by controlling degradation of regnase-1. Nat Immunol 12, 1167-1175.

Mathelier, A., Zhao, X., Zhang, A.W., Parcy, F., Worsley-Hunt, R., Arenillas, D.J., Buchman, S., Chen, C.Y., Chou, A., Ienasescu, H., et al. (2014). JASPAR 2014: an extensively expanded and updated open-access database of transcription factor binding profiles. Nucleic Acids Res 42, D142-147.

Matsushita, K., Takeuchi, O., Standley, D.M., Kumagai, Y., Kawagoe, T., Miyake, T., Satoh, T., Kato, H., Tsujimura, T., Nakamura, H., et al. (2009). Zc3h12a is an RNase essential for controlling immune responses by regulating mRNA decay. Nature 458, 1185-1190.

Mencacci, A., Cenci, E., Boelaert, J.R., Bucci, P., Mosci, P., Fe d'Ostiani, C., Bistoni, F., and Romani, L. (1997). Iron overload alters innate and T helper cell responses to Candida albicans in mice. J Infect Dis 175, 1467-1476.

Nowarski, R., Jackson, R., Gagliani, N., de Zoete, M.R., Palm, N.W., Bailis, W., Low, J.S., Harman, C.C., Graham, M., Elinav, E., et al. (2015). Epithelial IL-18 Equilibrium Controls Barrier Function in Colitis.

Cell 163, 1444-1456.

Shah, Y.M., Matsubara, T., Ito, S., Yim, S.H., and Gonzalez, F.J. (2009). Intestinal hypoxia-inducible transcription factors are essential for iron absorption following iron deficiency. Cell Metab 9, 152-164.

Shinkai, Y., Rathbun, G., Lam, K.P., Oltz, E.M., Stewart, V., Mendelsohn, M., Charron, J., Datta, M., Young, F., Stall, A.M., et al. (1992). RAG-2-deficient mice lack mature lymphocytes owing to inability to initiate V(D)J rearrangement. Cell 68, 855-867.

Takeda, K., Ho, V.C., Takeda, H., Duan, L.J., Nagy, A., and Fong, G.H. (2006). Placental but not heart defects are associated with elevated hypoxia-inducible factor alpha levels in mice lacking prolyl hydroxylase domain protein 2. Mol Cell Biol 26, 8336-8346.

Uehata, T., Iwasaki, H., Vandenbon, A., Matsushita, K., Hernandez-Cuellar, E., Kuniyoshi, K., Satoh, T., Mino, T., Suzuki, Y., Standley, D.M., et al. (2013). Malt1-induced cleavage of regnase-1 in CD4(+) helper T cells regulates immune activation. Cell 153, 1036-1049.

Zuker, M. (2003). Mfold web server for nucleic acid folding and hybridization prediction. Nucleic Acids Res 31, 3406-3415.